ChemPubSoc Europe

DOI: 10.1002/chem.201404856

CHEMISTRY A European Journal Full Paper

Palladium Complexes

# Insights into Functional-Group-Tolerant Polymerization Catalysis with Phosphine–Sulfonamide Palladium(II) Complexes

Zhongbao Jian,[a] Laura Falivene,[b] Philipp Wucher,[a] Philipp Roesle,[a] Lucia Caporaso,*[c] Luigi Cavallo,[b] Inigo Göttker-Schnetmann,[a] and Stefan Mecking*[a]

**Abstract:** Two series of cationic palladium(II) methyl complexes $\{[(2\text{-}MeOC_6H_4)_2PC_6H_4SO_2NHC_6H_3(2,6\text{-}R^1,R^2)]PdMe\}_2[A]_2$ ($^{X}$**1**$^{+}$**-A**: $R^1=R^2=H$: $^{H}$**1**$^{+}$**-A**; $R^1=R^2=CH(CH_3)_2$: $^{DIPP}$**1**$^{+}$**-A**; $R^1=H$, $R^2=CF_3$: $^{CF3}$**1**$^{+}$**-A**; **A** = $BF_4$ or $SbF_6$) and neutral palladium(II) methyl complexes $\{[(2\text{-}MeOC_6H_4)_2PC_6H_4SO_2NC_6H_3(2,6\text{-}R^1,R^2)]PdMe(L)\}$ ($^{X}$**1-acetone**: L = acetone; $^{X}$**1-dmso**: L = dimethyl sulfoxide; $^{X}$**1-pyr**: L = pyridine) chelated by a phosphine–sulfonamide were synthesized and fully characterized. Stoichiometric insertion of methyl acrylate (MA) into all complexes revealed that a 2,1 regiochemistry dominates in the first insertion of MA. Subsequently, for the cationic complexes $^{X}$**1**$^{+}$**-A**, β-H elimination from the 2,1-insertion product $^{X}$**2**$^{+}$**-A**$_{MA\text{-}2,1}$ is overwhelmingly favored over a second MA insertion to yield two major products $^{X}$**4**$^{+}$**-A**$_{MA\text{-}1,2}$ and $^{X}$**5**$^{+}$**-A**$_{MA}$. By contrast, for the weakly coordinated neutral complexes $^{X}$**1-acetone** and $^{X}$**1-dmso**, a second MA insertion of the 2,1-insertion product $^{X}$**2**$_{MA\text{-}2,1}$ is faster than β-H elimination and gives $^{X}$**3**$_{MA}$ as major products. For the strongly coordinated neutral complexes $^{X}$**1-pyr**, no second MA insertion and no β-H elimination (except for $^{DIPP}$**2-pyr**$_{MA\text{-}2,1}$) were observed for the 2,1-insertion product $^{X}$**2-pyr**$_{MA\text{-}2,1}$. The cationic complexes $^{X}$**1**$^{+}$**-A** exhibited high catalytic activities for ethylene dimerization, affording butenes ($C_4$) with a high selectivity of up to 97.7% (1-butene: 99.3%). Differences in activities and selectivities suggest that the phosphine–sulfonamide ligands remain coordinated to the metal center in a bidentate fashion in the catalytically active species. By comparison, the neutral complexes $^{X}$**1-acetone**, $^{X}$**1-dmso**, and $^{X}$**1-pyr** showed very low activity towards ethylene to give traces of oligomers. DFT analyses taking into account the two possible coordination modes (O or N) of the sulfonamide ligand for the cationic system $^{CF3}$**1**$^{+}$ suggested that the experimentally observed high activity in ethylene dimerization is the result of a facile first ethylene insertion into the O-coordinated PdMe isomer and a subsequent favored β-H elimination from the N-coordinated isomer formed by isomerization of the insertion product. Steric hindrance by the *N*-aryl substituent in the neutral systems $^{CF3}$**1** and $^{H}$**1** appears to contribute significantly to a higher barrier of insertion, which accounts for the experimentally observed low activity towards ethylene oligomerization.

## Introduction

Late-transition-metal catalysts have been intensively studied for olefin oligomerization and copolymerization, due to their different incorporation behavior, branch formation, and generally less oxophilic nature.[1–5] Among them, palladium catalysts are of advantage for the insertion copolymerization of polar vinyl monomers. Since the finding by Brookhart and co-workers that cationic $Pd^{II}$ diimine catalysts can catalyze the insertion copolymerization of ethylene or 1-olefins and acrylates,[6] many studies on insertion polymerization have focused on $Pd^{II}$ catalysts chelated by various ligands. Another significant breakthrough was reported by Drent and co-workers, who revealed that a neutral phosphinesulfonato palladium species could produce highly linear copolymers of ethylene and methyl acrylate (MA).[7] In the past decade, this phosphinesulfonato $Pd^{II}$ catalyst has been found to promote the formation of linear copolymers of ethylene with a broad scope of polar monomers including not only acrylates, but also acrylonitrile, vinyl acetate, vinyl ether, vinyl fluoride, vinyl chloride, allylic monomers, acrylic acid, and acrylamides.[8,9] An important structural feature of catalysts containing phosphine–sulfonates (**A**), which renders them capable of insertion chain growth, is the presence of one hard sulfonate oxygen and one soft phosphine σ-donor ligand.[9h] The phosphinesulfonato catalyst system was long considered to be unique in ethylene/polar vinyl monomer copolymerization to give linear copolymer. Recently, Nozaki and co-workers reported a series of cationic phosphine/phosphine

[a] Dr. Z. Jian, P. Wucher, P. Roesle, Dr. I. Göttker-Schnetmann, Prof. Dr. S. Mecking
Chair of Chemical Materials Science, Department of Chemistry
University of Konstanz, 78464 Konstanz (Germany)
E-mail: Stefan.Mecking@uni-konstanz.de

[b] Dr. L. Falivene, Prof. Dr. L. Cavallo
Physical Sciences and Engineering, Kaust Catalysis Center
King Abdullah University of Science and Technology (KAUST)
Thuwal 23955-6900 (Saudi Arabia)

[c] Dr. L. Caporaso
Department of Chemistry and Biology, University of Salerno
Via Giovanni Paolo II, 132-84084, Fisciano (SA) (Italy)
E-mail: lcaporaso@unisa.it

Supporting information for this article is available on the WWW under http://dx.doi.org/10.1002/chem.201404856.

monoxide complexes **B** that catalyze linear copolymerization of ethylene with a range of polar vinyl monomers.[10] This important finding shows that the phosphinesulfonato motif is not unique. Beyond the above insights, an understanding of the criteria for a ligand environment that promotes insertion chain growth and copolymerization is lacking to date. To shed light on this case, we chose the phosphine–sulfonamide motif (**C** and **D**) for a combined experimental and theoretical study.[11] This allows for the formation of cationic and neutral palladium(II) complexes with one ligand system coordinating through different hard donors (N/O), and at the same time the introduction of steric bulk at the hard donor by means of *N*-aryl moieties.

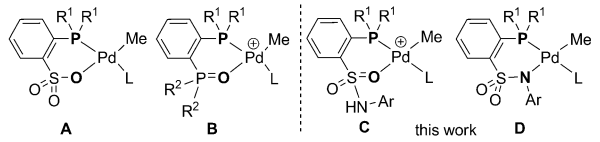


## Results and Discussion

### Synthesis of phosphine–sulfonamide ligands and cationic palladium(II) complexes

Phosphine–sulfonamides **La**–**c** were synthesized by modified literature procedures.[7] Treatment of sulfonamides with two equivalents of *n*BuLi at room temperature for 2 h, followed by in situ reaction with $(2\text{-MeOC}_6H_4)_2PCl$ at 50 °C for a further 12 h, afforded the lithium phosphine–sulfonamide salts, which were protonated to give **La**–**c** as colorless or pale yellow crystals in 47–63% yield (Scheme 1). Ligands **La**–**c** were fully characterized by multinuclear NMR spectroscopy ($^1H$, $^{13}C$, and $^{31}P$), X-ray diffraction, and elemental analysis. Generally, as a consequence of the $pK_a$ values of $ArSO_3H$ (e.g., $pK_a(PhSO_3H) = -2.8$) and $Ar_3P^+H$ ($pK_a \leq 2.7$),[12] the phosphine–sulfonic acids are usually zwitterionic compounds in which the acidic proton is located at the phosphorus atom, as evidenced by both the coupling constant ($^1J_{PH} \approx 600$ Hz) and the chemical shift ($\delta \approx 9.0$ ppm).[7] As expected from the large $pK_a$ value of $ArSO_2NHR$ (e.g., $pK_a(PhSO_2NH_2) = 10.1$), we did not observe any similar signals in the $^1H$ NMR spectra of **La**–**c**, but the signals found around 8.14, 7.35, and 8.35 ppm, respectively, could be assigned to the NH proton. Moreover, this is also exemplified by the solid-state structure of the phosphine–sulfonamide **Lb**, in which H33 is located at the nitrogen atom with a bond length of about 0.82 Å ($d$(P1—H33) ≈ 2.70 Å, Figure 1).

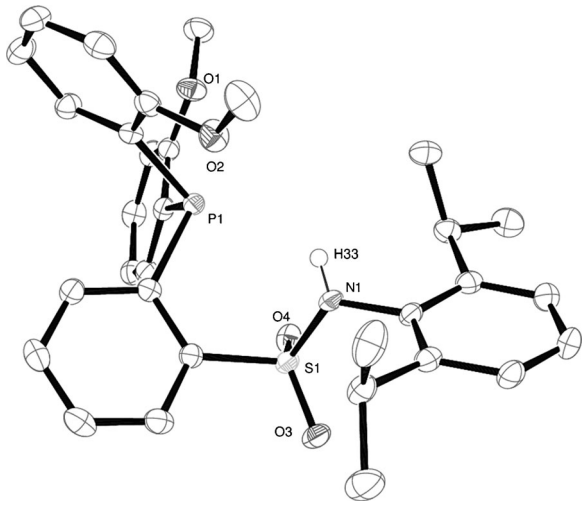


**Figure 1.** ORTEP of ligand **Lb** drawn with 50% probability ellipsoids. Hydrogen atoms (except NH) are omitted for clarity.

Phosphine–sulfonamides **La**–**c** react readily with one equivalent of [PdMeCl(cod)] at room temperature to straightforwardly generate the desired neutral $Pd^{II}$ complexes $^{X}$**1-Cl**, which were isolated in satisfactory yields of 62–69% (Scheme 1). The $^1H$ NMR spectra of $^{X}$**1-Cl** suggest that the NH group in the ligand is not deprotonated during the reaction, but 1,5-cyclooctadiene (cod) is replaced by the intact neutral ligand. The NH protons in $^{X}$**1-Cl** are unambiguously observed at $\delta = 8.50$, 8.68, and 8.38 ppm, respectively. In addition, doublets at $\delta =$ 0.57, 0.96, and 0.76 ppm arising from coupling to phosphorus ($^3J_{PH}$) can be assigned to the PdMe group (Table 1). On the basis of NMR spectroscopic data, one cannot differentiate unambiguously between a $\kappa^2$-*P,O* and a $\kappa^2$-*P,N* bidentate coordination mode in $^{X}$**1-Cl**, and hence the solid-state structure was determined by X-ray diffraction. Suitable crystals of $^{DIPP}$**1-Cl** were grown by layering a $CH_2Cl_2$ solution of the complex with pentane. X-ray diffraction analysis of $^{DIPP}$**1-Cl** revealed that the formally neutral phosphine–sulfonamide ligand coordinates to the Pd center in a $\kappa^2$-*P,O* fashion, and H34 is located at the nitrogen atom (Figure 2). The Pd1—P1

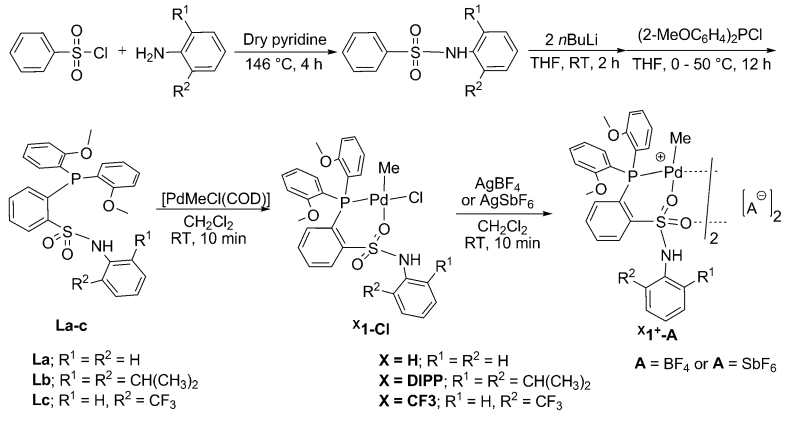


**Scheme 1.** Synthesis of phosphine–sulfonamide ligands **La**–**c** and cationic $Pd^{II}$ complexes $^{X}$**1**$^{+}$**-A**.

**Table 1.** Selected chemical shifts [ppm] of palladium complexes.

| | $^{1}$H (PdMe) | $^{13}$C (PdMe) | $^{31}$P |
|---|---|---|---|
| $^{H}$**1-Cl** | 0.57 (d) | – | 23.2 |
| $^{DIPP}$**1-Cl** | 0.96 (d) | 1.62 (s) | 20.8 |
| $^{CF3}$**1-Cl** | 0.76 (d) | 2.44 (s) | 21.9 |
| $^{H}$**1**$^{+}$**-BF$_4$** | 0.65 (s) | 8.24 (d) | 28.6 |
| $^{H}$**1**$^{+}$**-SbF$_6$** | 0.67 (s) | 7.96 (s) | 26.6 |
| $^{DIPP}$**1**$^{+}$**-BF$_4$** | 0.71 (s) | 6.62 (s) | 24.0 |
| $^{DIPP}$**1**$^{+}$**-SbF$_6$** | 0.55 (s) | 6.36 (s) | 24.5 |
| $^{CF3}$**1**$^{+}$**-BF$_4$** | 0.76 (s) | 8.41 (s) | 25.3 |
| $^{CF3}$**1**$^{+}$**-SbF$_6$** | 0.73 (s) | 7.54 (s) | 23.7 |
| $^{DIPP}$**1-acetone** | −0.20 (s) | 1.59 (s) | 28.3 |
| $^{DIPP}$**1-dmso** | −0.12 (s) | 2.02 (d) | 29.4 |
| $^{CF3}$**1-acetone** | −0.17 (s) | 1.61 (s) | 28.3 |
| $^{CF3}$**1-dmso** | −0.03 (s) | 2.52 (s) | 26.7 |
| $^{H}$**1-pyr** | −0.04 (d) | 0.99 (d) | 23.5 |
| $^{DIPP}$**1-pyr** | −0.20 (d) | 2.25 (d) | 24.1 |
| $^{CF3}$**1-pyr** | −0.18 (d) | 0.17 (d) | 24.4 |

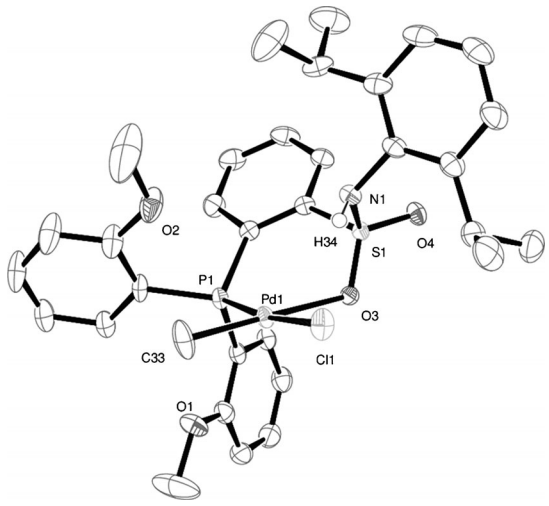


**Figure 2.** ORTEP of complex $^{DIPP}$**1-Cl** drawn with 50% probability ellipsoids. Hydrogen atoms (except NH) are omitted for clarity. Selected bond lengths [Å]: Pd1–O3 2.249(2), Pd1–P1 2.216(6), Pd1–C33 2.005(3), Pd1–Cl1 2.362(6).

distance (2.216(6) Å) is slightly shorter than in the analogous phosphinesulfonato Pd$^{II}$ complex [{(*o*-(*o*-MeOC$_6$H$_4$)$_2$P)-C$_6$H$_4$SO$_3$}PdMe(lutidine)] (2.234(9) Å),[9l] whereas the Pd1–O3 distance (2.249(2) Å) is significantly longer than the Pd–O distance (2.159(2) Å).[9l] In addition, the Pd1–C33 distance (2.005(3) Å) is within the range of typical Pd–C bonds. To study the strength of the Pd–O bond in $^{X}$**1-Cl**, we added an excess of a coordinating solvent such as acetone or DMSO to $^{X}$**1-Cl**. However, $^{1}$H NMR signals remained unaltered, that is, the chelating Pd–O coordination in $^{X}$**1-Cl** is stronger than the binding strength between Pd and acetone or DMSO.

The palladium complexes $^{X}$**1-Cl** further reacted with silver(I) salts ($AgBF_4$ or $AgSbF_6$) in $CH_2Cl_2$ to generate the cationic palladium(II) methyl complexes $^{X}$**1**$^{+}$**-A** (A = $BF_4$ and $SbF_6$) in good yields (Scheme 1). Complexes $^{X}$**1**$^{+}$**-BF$_4$** and $^{X}$**1**$^{+}$**-SbF$_6$** were fully identified by 1D ($^{1}$H, $^{13}$C, $^{19}$F, and $^{31}$P) and 2D NMR spectroscopy and elemental analysis. The methyl protons of the PdMe group in all cationic complexes were clearly observed between 0.55 and 0.76 ppm (Table 1). Because the reaction took place in a noncoordinating solvent, we inferred that $^{X}$**1**$^{+}$**-BF$_4$** and $^{X}$**1**$^{+}$**-SbF$_6$** have dimeric structures in which the fourth coordination site at the Pd$^{II}$ center is occupied by a sulfonamide group of the second [(PSO$_2$NHAr)PdMe] fragment. Analogous dimers have been reported for different phosphinesulfonato Pd$^{II}$ complexes.[9a,13]

### Decomposition of cationic palladium(II) methyl complexes

To confirm the structures of cationic Pd$^{II}$ methyl complexes $^{X}$**1**$^{+}$**-A**, we attempted to isolate crystals suitable for X-ray diffraction analysis. For example, by layering a $CD_2Cl_2$ solution of $^{DIPP}$**1**$^{+}$**-SbF$_6$** with pentane (Scheme 2), red crystals suitable for

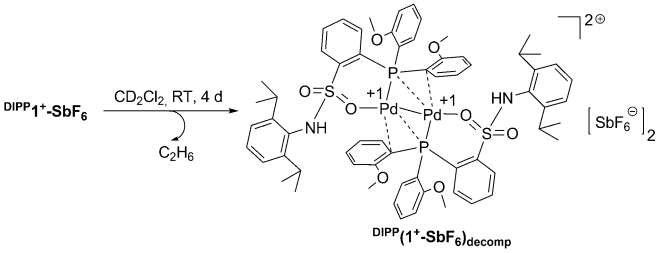


**Scheme 2.** Formation of binuclear cationic Pd$^{I}$ complex $^{DIPP}$**(1**$^{+}$**-SbF$_6$)$_{decomp.}$**.

X-ray diffraction were obtained within 4 d. X-ray diffraction analysis revealed that these crystals were not the target complex $^{DIPP}$**1**$^{+}$**-SbF$_6$**, but the decomposition product $^{DIPP}$**(1**$^{+}$**-SbF$_6$)$_{decomp.}$**. As reported previously, the decomposition of a phosphinesulfonato Pd$^{II}$ methyl complex usually generates Pd$^{0}$ black and Pd$^{II}$L$_2$ or free ligand.[14] However, $^{DIPP}$**(1**$^{+}$**-SbF$_6$)$_{decomp.}$**, formed by the decomposition of cationic Pd$^{II}$ methyl complex $^{DIPP}$**1**$^{+}$**-SbF$_6$**, is a binuclear cationic Pd$^{I}$ complex with a Pd$^{I}$–Pd$^{I}$ bond (Figure 3). A protonated NH moiety was

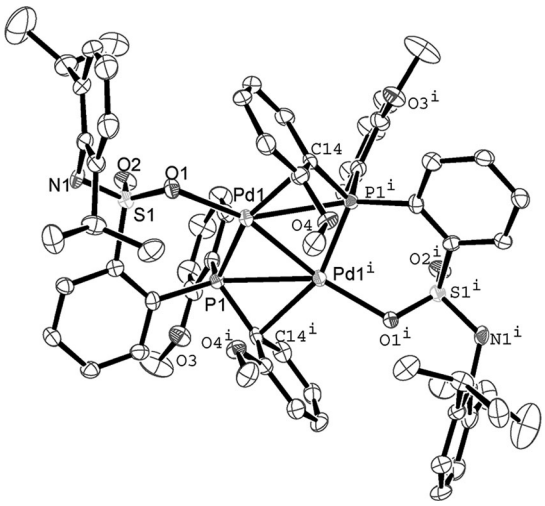


**Figure 3.** ORTEP of complex $^{DIPP}$**(1**$^{+}$**-SbF$_6$)$_{decomp.}$** drawn with 50% probability ellipsoids. Hydrogen atoms, cocrystallized solvent molecules, and $SbF_6$ anion are omitted for clarity. Selected bond lengths [Å]: Pd1–O1 2.157(5), Pd1–P1 2.198(2), Pd1–P1$^{i}$ 2.758(2), Pd1–C14 2.326(7), Pd1–Pd1$^{i}$ 2.544(1).

found in the electron density map by X-ray diffraction. An analogous reaction pathway has been observed in $Pd^{II}$ zwitterion $[(Ph_2B(PPh_2)_2)PdMe(thf)]$, which can also generate red $Pd^{I}$–$Pd^{I}$ dimer $[\{(Ph_2B(PPh_2)_2)Pd\}_2]$ on addition of $H_2$.[15] The neutral phosphine–sulfonamide ligand coordinates to one Pd center in a $\kappa^2$-*P,O* bidentate mode, and to another Pd center in a weak $\eta^2$-*P,C* fashion (Pd1–$P1^{i}$ 2.758(2), Pd1–C14 = 2.326(7) Å).[15] The $Pd^{I}$–$Pd^{I}$ distance of 2.544(1) Å in $^{DIPP}(\mathbf{1}^{+}\text{-}\mathbf{SbF_6})_{decomp.}$ is close to that in $[Pd_2(NPN\text{-}NPN)_2](BF_4)_2$ (2.5489(7) Å),[16a] but slightly shorter than those in $[Pd^{I}_2(\mu\text{-}2\text{-}C_6F_4PPh_2)_2(L)_2]$ (L = $PPh_3$, 2.5740(3) Å; L = $AsPh_3$, 2.5511(3) Å; L = *t*BuNC, 2.5803(4) Å)[16b] and much shorter than that in $[\{(Ph_2B(PPh_2)_2)Pd\}_2]$ (2.728(6) Å).[15]

### Synthesis of neutral palladium(II) methyl complexes

By addition of NaH to phosphine–sulfonamides **La–c**, the sodium salts **La–c-Na** were readily obtained in high yields. **Lb**,**c-Na** reacted with [PdMeCl(cod)] in acetone and $CH_2Cl_2$ to readily afford the neutral $Pd^{II}$ methyl complexes $^{X}$**1-acetone** in good yields (Scheme 3). In comparison with the cationic $Pd^{II}$ complexes $^{X}\mathbf{1}^{+}$**-A**, the signals of the PdMe group in the $^1$H NMR spectra of $^{X}$**1-acetone** are shifted upfield to −0.20 and −0.17 ppm, respectively (Table 1). In addition, the coordinated acetone molecule gives rise to a strong singlet at $\delta = 1.97$ and 2.20 ppm, respectively. As reported previously, the same reaction of sodium salt of phosphine–sulfonate [(PO)Na] with [PdMeCl(COD)] always yielded the dimer $[(\{(PO)Pd(Me)Cl\}\mu\text{-}Na(acetone)_2)_2]$, in which the Cl atom is bound to the Pd center.[17] Strongly coordinating solvents such as pyridine or silver salts are necessary to abstract the Cl atom. However, X-ray studies unambiguously revealed that acetone directly binds to the palladium center with a reasonable Pd–O distance in $^{X}$**1-acetone**, and the phosphine–sulfonamide ligand coordinates to the palladium center in a $\kappa^2$-*P,N* fashion (Figure 4). The

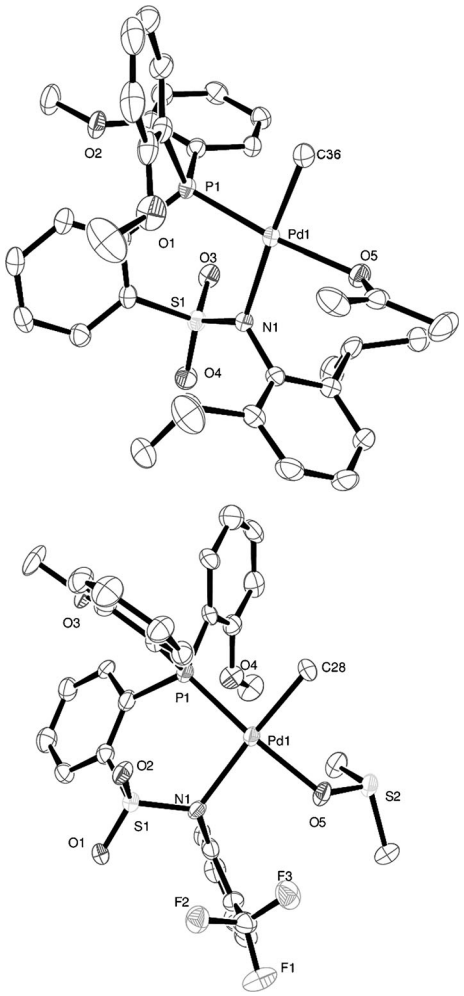


**Figure 4.** ORTEPs of neutral complexes $^{DIPP}$**1-acetone** and $^{CF3}$**1-dmso** drawn with 50% probability ellipsoids. Hydrogen atoms and cocrystallized solvent molecules are omitted for clarity.

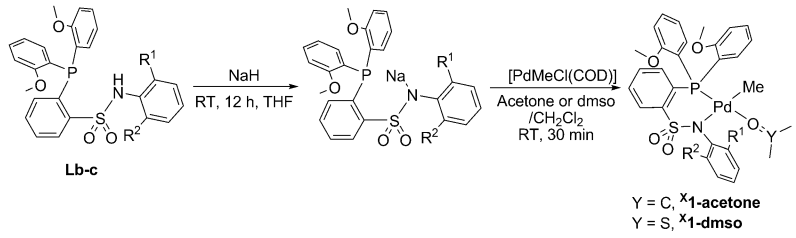


**Scheme 3.** Synthesis of neutral $Pd^{II}$ methyl complexes $^{X}$**1-acetone** and $^{X}$**1-dmso**.

Pd1–O5(acetone) bond (2.148(2) Å) is longer than the Pd–O(dmso) bonds in [(PO)Pd(Me)(dmso)] (2.131(2)–2.146(3) Å),[9a,18] that is, acetone is a more weakly coordinating solvent than DMSO (see below, Table 2). To the best of our knowledge, this is the first structurally characterized palladium complex directly coordinated by a weakly binding acetone ligand. In addition, by replacement of acetone with DMSO as a solvent in the reaction of **Lb**,**c-Na** and [PdMeCl(COD)], complexes $^{X}$**1-dmso** were obtained in high yields, which could be accessed alternatively by addition of dmso to $^{X}$**1-acetone** (Scheme 3). Generally, DMSO can coordinate to the $Pd^{II}$ center in the palladium complexes in a $\kappa^1$-*O* or a $\kappa^1$-*S* mode.[9a,k,18] In this case, X-ray diffraction revealed that DMSO binds to the palladium center in a $\kappa^1$-*O* mode (Figure 4). The Pd1–O5 bond length (2.136(4) Å) in $^{CF3}$**1-dmso** is reasonably shorter than the Pd1–O5 bond length of 2.148(2) Å in $^{DIPP}$**1-acetone** (Table 2).

Nozaki and co-workers reported that treatment of a phosphine–sulfonate ligand with 2,6-lutidine followed by addition of [PdMeCl(cod)] affords the neutral $Pd^{II}$ complex $[\{(o\text{-}(o\text{-}MeOC_6H_4)_2P)C_6H_4SO_3\}PdMe(lutidine)]$.[9l] In this case, the reactions of phosphine–sulfonamide ligands **La–c** and pyridine did not take place owing to the large p$K_a$ value of sulfonamide; however, treatment of $Pd^{II}$ complexes $^{X}$**1-Cl** with pyridine generated the neutral $Pd^{II}$ methyl complexes $^{X}$**1-pyr**, which could

**Table 2.** Selected bond lengths [Å] for neutral palladium complexes.

| | $^{DIPP}$**1-acetone** | $^{CF3}$**1-dmso** | $^{H}$**1-pyr** | $^{DIPP}$**1-pyr** | $^{CF3}$**1-pyr** |
|---|---|---|---|---|---|
| Pd–C | 2.041(2) | 2.051(6) | 2.097(2) | 2.051(2) | 2.046(2) |
| Pd–N1 | 2.137(2) | 2.162(5) | 2.131(2) | 2.155(2) | 2.155(1) |
| Pd–O5/N2 | 2.148(2) | 2.136(4) | 2.132(2) | 2.118(2) | 2.120(2) |
| Pd–P | 2.208(5) | 2.203(2) | 2.236(6) | 2.248(6) | 2.228(4) |

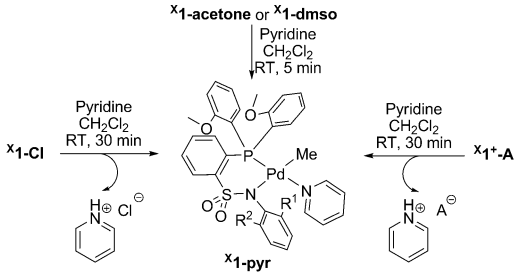


**Scheme 4.** Synthesis of neutral Pd$^{II}$ methyl complexes $^{X}$**1-pyr**.

also be obtained by adding pyridine to the cationic Pd$^{II}$ methyl complexes $^{X}$**1$^{+}$-A** (Scheme 4). In fact, $^{X}$**1-pyr** could be generated by addition of pyridine to the neutral Pd$^{II}$ methyl complexes $^{X}$**1-acetone** and $^{X}$**1-dmso** as well. The formation of $^{X}$**1-pyr** indicated that pyridine is capable of promoting deprotonation of the sulfonamide group in the palladium complexes. The $^{1}$H NMR spectra of $^{X}$**1-pyr** clearly revealed the absence of the NH hydrogen atom and the appearance of coordinated pyridine. The signals of the PdMe group in $^{X}$**1-pyr** are shifted upfield to −0.04, −0.20, and −0.18, respectively (Table 1). The solid-state structures of $^{X}$**1-pyr** were determined by X-ray crystallography. The PdMe group and the P atom are located *cis* to each other in the square-planar coordination sphere around the palladium center (Figure 5). The anionic phosphine–sulfonamide ligands coordinate to the palladium center in a $\kappa^2$-*P,N* bidentate mode. The Pd–C(Me) bond lengths (2.046(2)–2.097(2) Å) are in the expected range for Pd$^{II}$ methyl complexes (Table 2).[9]

## Stoichiometric insertion of methyl acrylate

The insertion of MA is one of the best-studied reactions of the prototypical $\kappa^2$-*P,O* Pd$^{II}$ complexes.[9,18,19] We have reported that the first insertion reaction of dianisyl phosphinesulfonato Pd$^{II}$ complexes $^{PSO3}$**1′-NaCl** and $^{PSO3}$**1′-dmso** with MA takes place primarily in a 2,1 mode, and then the 2,1-insertion product $^{PSO3}$**2′$_{MA\text{-}2,1}$** can undergo β-H elimination to give methyl crotonate or insert another molecule of MA to form the double-insertion product $^{PSO3}$**3′$_{MA}$** [Eq. (1)].[9k,19] Note that the second insertion step is predominant over β-H elimination from $^{PSO3}$**2′$_{MA\text{-}2,1}$**.[9b,19] The electronic and steric effects of the phosphine–sulfonate on the insertion reactions have been studied extensively, but a clear and general picture was not obtained.[9b,18,19a,b]

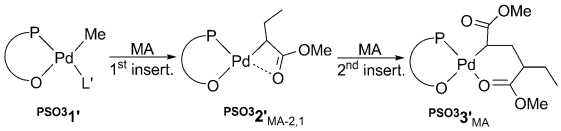


(1)

### *Insertion into cationic complexes*

For the evaluation of the reactivity of the complexes toward MA, the insertion reactions of an excess of MA (ca. 20 equiv) with cationic complexes $^{X}$**1$^{+}$-A** were monitored by $^{1}$H NMR spectroscopy at 25 °C over a period of 6–15 h (Supporting Information, Figure S32–S42). Insertion products (Scheme 5) were identified through assignment of their spin systems by $^{1}$H,$^{1}$H COSY and $^{1}$H,$^{1}$H TOCSY experiments, as well as by $^{1}$H,$^{13}$C HSQC experiments if required. Under these pseudo-first-order conditions, the first insertion of MA into the Pd–Me bond to give the first insertion product $^{X}$**2$^{+}$-A$_{MA}$** is fast at 25 °C for all cationic complexes and is complete within about 30 min. The

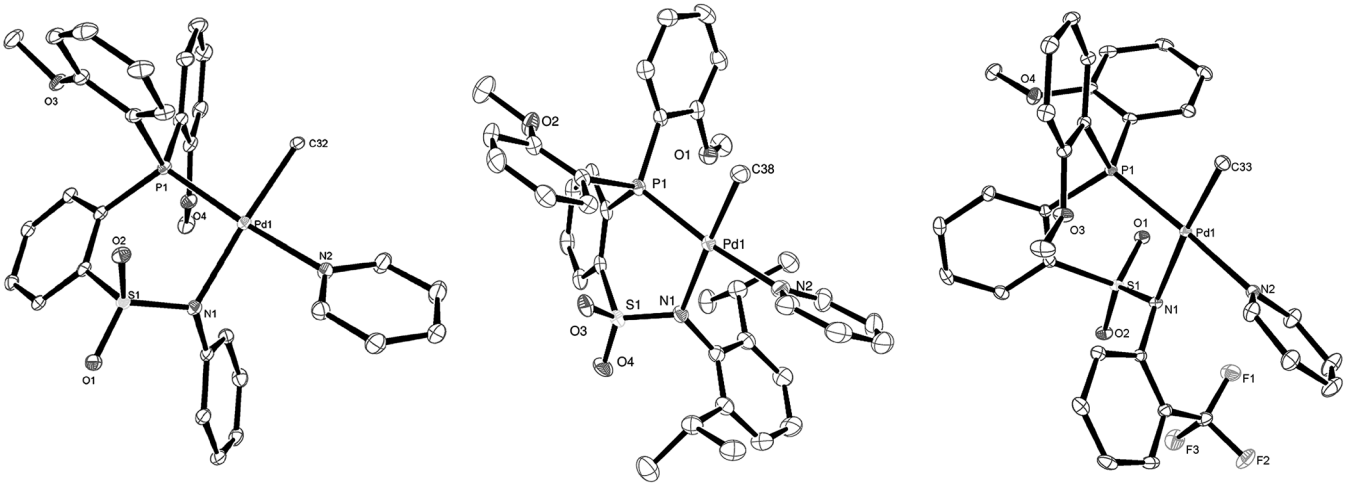


**Figure 5.** ORTEPs of neutral complexes $^{X}$**1-pyr** drawn with 50% probability ellipsoids. Hydrogen atoms and cocrystallized solvent molecules are omitted for clarity.

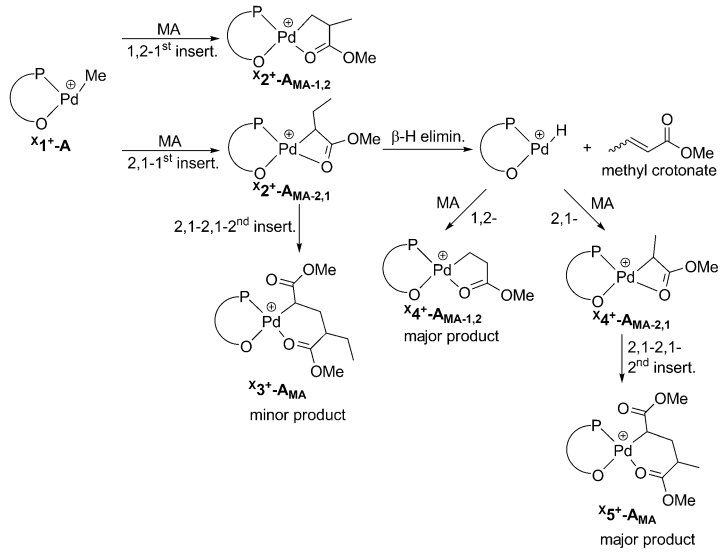


**Scheme 5.** Reaction of MA with cationic Pd$^{II}$ complexes $^{X}$**1**$^{+}$-**A**.

net rate constants $k_{1st}$ of the first insertion are in the range (2.0–3.5)$\times10^{-3}$ s$^{-1}$ (Table 3, runs 1–6),[20] which is close to the rate constant for $^{PSO3}$**1′-NaCl** ($k_{1st}=3.2\times10^{-3}$ s$^{-1}$ at 25 °C).[19a] The observed ratios of 2,1 to 1,2 regioselectivity in the first insertion product are about 10:1, 6:1, and 11:1 for $^{H}$**1**$^{+}$-**A**, $^{DIPP}$**1**$^{+}$-**A**, and $^{CF3}$**1**$^{+}$-**A** respectively. This is in agreement with the trend that the 2,1 mode generally dominates in the first insertion step for phosphinesulfonato Pd$^{II}$ methyl complexes. In the next step, the second insertion of MA into the minor, 1,2-insertion product $^{X}$**2**$^{+}$-**A**$_{MA-1,2}$ is generally inhibited, because of the formation of a stable five-membered chelate, but the second insertion of MA and/or the β-H elimination occur in the major, 2,1-insertion product $^{X}$**2**$^{+}$-**A**$_{MA-2,1}$. Notably, in comparison with the relatively small rate constant for β-H elimination ($k_{\beta H-1st}=1.0\times10^{-5}$ s$^{-1}$) of $^{PSO3}$**2′**$_{MA-2,1}$, which is one order of magnitude smaller than the rate constant for the second MA insertion ($k_{2nd}=9.2\times10^{-5}$ s$^{-1}$) of $^{PSO3}$**2′**$_{MA-2,1}$,[19a] analogous β-H elimination rate constants in all cationic complexes $^{X}$**1**$^{+}$-**A** are two orders of magnitude higher. The largest $k_{\beta H-1st}$ is up to $280\times10^{-5}$ s$^{-1}$ (Table 3, run 4), and thus β-H elimination is overwhelmingly favored over the second MA insertion for $^{X}$**2**$^{+}$-**A**$_{MA-2,1}$. A typical $^{1}$H NMR analysis is depicted in Figure 6. The prominent doublet of doublets (dd, $^{3}J_{HH}=7.2$, $^{4}J_{HH}=2.0$ Hz, *trans*-Me) at $\delta=1.86$ ppm is assigned to *trans*-methyl crotonate, which results from the β-H elimination of $^{CF3}$(**2**$^{+}$-**SbF$_6$**)$_{MA-2,1}$. The observed two major products $^{CF3}$(**4**$^{+}$-**SbF$_6$**)$_{MA-1,2}$ and $^{CF3}$(**5**$^{+}$-**SbF$_6$**)$_{MA}$ (*rac*:*meso*=6:5) originate from single 1,2 insertion or two consecutive 2,1 insertions of MA into the intermediate PdH species, respectively.[22] The observed ratio of 2,1 to 1,2 regioselectivity in the second MA insertion is about 3:1, which is lower than that of MA insertion into the Pd–Me bond (11:1). A different regioselectivity for MA insertion into PdH and PdMe groups has also been found in diazaphospholidinesulfonato Pd$^{II}$ complexes.[18a] In conclusion, the ratio of insertion products $^{CF3}$(**5**$^{+}$-**SbF$_6$**)$_{MA}$/$^{CF3}$(**4**$^{+}$-**SbF$_6$**)$_{MA-1,2}$/$^{CF3}$(**2**$^{+}$-**SbF$_6$**)$_{MA-1,2}$/$^{CF3}$(**3**$^{+}$-**SbF$_6$**)$_{MA}$ is about 65:23:9:3, which differs strongly from the product distribution of MA insertion into $^{PSO3}$**1′**, in which $^{PSO3}$**3′**$_{MA}$ is the major product. This shows again that β-H elimination is considerably favored for these cationic complexes $^{X}$**1**$^{+}$-**A**.

**Table 3.** Rate constants of first insertion and β-H elimination and regioselectivity.[a]

| Run | Catalyst | $10^3 k_{1st}$ [s$^{-1}$] | $10^5 k_{\beta H-1st}$ [s$^{-1}$] | Regioselectivity 2,1:1,2- |
|---|---|---|---|---|
| 1 | $^{H}$**1**$^{+}$-**BF$_4$** | 2.0 | 63 | ≈10:1[b] |
| 2 | $^{H}$**1**$^{+}$-**SbF$_6$** | 2.2 | 180 | 10:1 |
| 3 | $^{DIPP}$**1**$^{+}$-**BF$_4$** | 3.5 | ≈220[b] | 6:1 |
| 4 | $^{DIPP}$**1**$^{+}$-**SbF$_6$** | 3.3 | 280 | 6:1 |
| 5 | $^{CF3}$**1**$^{+}$-**BF$_4$** | ≈3.1[b] | 83 | 11:1 |
| 6 | $^{CF3}$**1**$^{+}$-**SbF$_6$** | ≈3.0[b] | 180 | 11:1 |
| 7 | $^{PSO3}$**1′-NaCl**[c] | 3.2 | 1.0 | >15:1 |
| 8 | $^{DIPP}$**1-acetone** | >100 | 2.1 | ≈7:1[b] |
| 9 | $^{CF3}$**1-acetone** | >80 | 2.2 | 12:1 |
| 10 | $^{PSO3}$**1′-dmso** | 0.7 | 2.1 | 20:1 |
| 11 | $^{DIPP}$**1-dmso** | 11 | ≈1.5[b] | ≈7:1[b] |
| 12 | $^{CF3}$**1-dmso** | 3.8 | 3.0 | ≈12:1[b] |
| 13 | $^{H}$**1-pyr** | 0.003 | n.o.[d] | 2,1[e] |
| 14 | $^{DIPP}$**1-pyr** | 0.005 | n.o.[d] | 2,1[e] |
| 15 | $^{CF3}$**1-pyr** | 0.0001 | n.o.[d] | 2,1[e] |
| 16 | $^{PSO3}$**1′-pyr**[f] | 0.012 | ≈1.8[b] | 2,1[e] |
| 17 | $^{H}$**1-pyr**[f] | 0.045 | n.o.[d] | 2,1[e] |
| 18 | $^{DIPP}$**1-pyr**[f] | 0.048 | ≈0.6[b] | 2,1[e] |
| 19 | $^{CF3}$**1-pyr**[f] | 0.013 | n.o.[d] | 2,1[e] |

[a] Conditions: Pd (0.025 mol L$^{-1}$), MA (20 equiv), $CD_2Cl_2$, $T=25$ °C, unless otherwise noted. [b] Exact determination not possible due to overlapping or broad resonances. [c] By addition of 1.1 equiv $AgBF_4$, ref. [19a]. [d] No β-H elimination observed. [e] No first 1,2 insertion product observed due to the low intensity. [f] $C_2D_2Cl_4$, $T=50$ °C.

### *Insertion into weakly coordinated neutral complexes*

The above findings suggested studies on the analogous MA insertions for the neutral $\kappa^2$-P,N complexes $^{X}$**1-acetone** and $^{X}$**1-dmso**. The reactions of an excess of MA (ca. 20 equiv) with the neutral complexes $^{X}$**1-acetone** and $^{X}$**1-dmso** were monitored by $^{1}$H NMR spectroscopy at 25 °C over a period of 13–15 h (Supporting Information, Figures S45–S49). Kinetic experiments revealed that the first insertion of MA into the Pd–Me bond is fast. Especially for $^{DIPP}$**1-acetone**, the insertion is complete within about 5 min. Note that the observed rate constants $k_{1st}$ are a combination of the pre-equilibrium $^{X}$**1**-solvent + MA⇌$^{X}$**1**-MA + solvent (solvent = acetone or dmso) and the actual rate of insertion for $^{X}$**1**-MA. Under the pseudo-first-order conditions, the weakly coordinated acetone complex $^{X}$**1-acetone** undergoes the fastest insertion of MA into the Pd–Me bond ($k_{1st}>(80–100)\times10^{-3}$ s$^{-1}$), which is significantly faster than those for $^{PSO3}$**1′-NaCl** ($k_{1st}=3.2\times10^{-3}$ s$^{-1}$) and dmso complexes $^{PSO3}$**1′-dmso** ($k_{1st}=0.7\times10^{-3}$ s$^{-1}$) and $^{X}$**1-dmso** ($k_{1st}=11\times10^{-3}$ and $3.8\times10^{-3}$ s$^{-1}$; Table 3), which suggests that weakly coordinated acetone is easily dissociated from the palladium center in the presence of MA. The observed ratios of 2,1 to 1,2 regioselectiv-

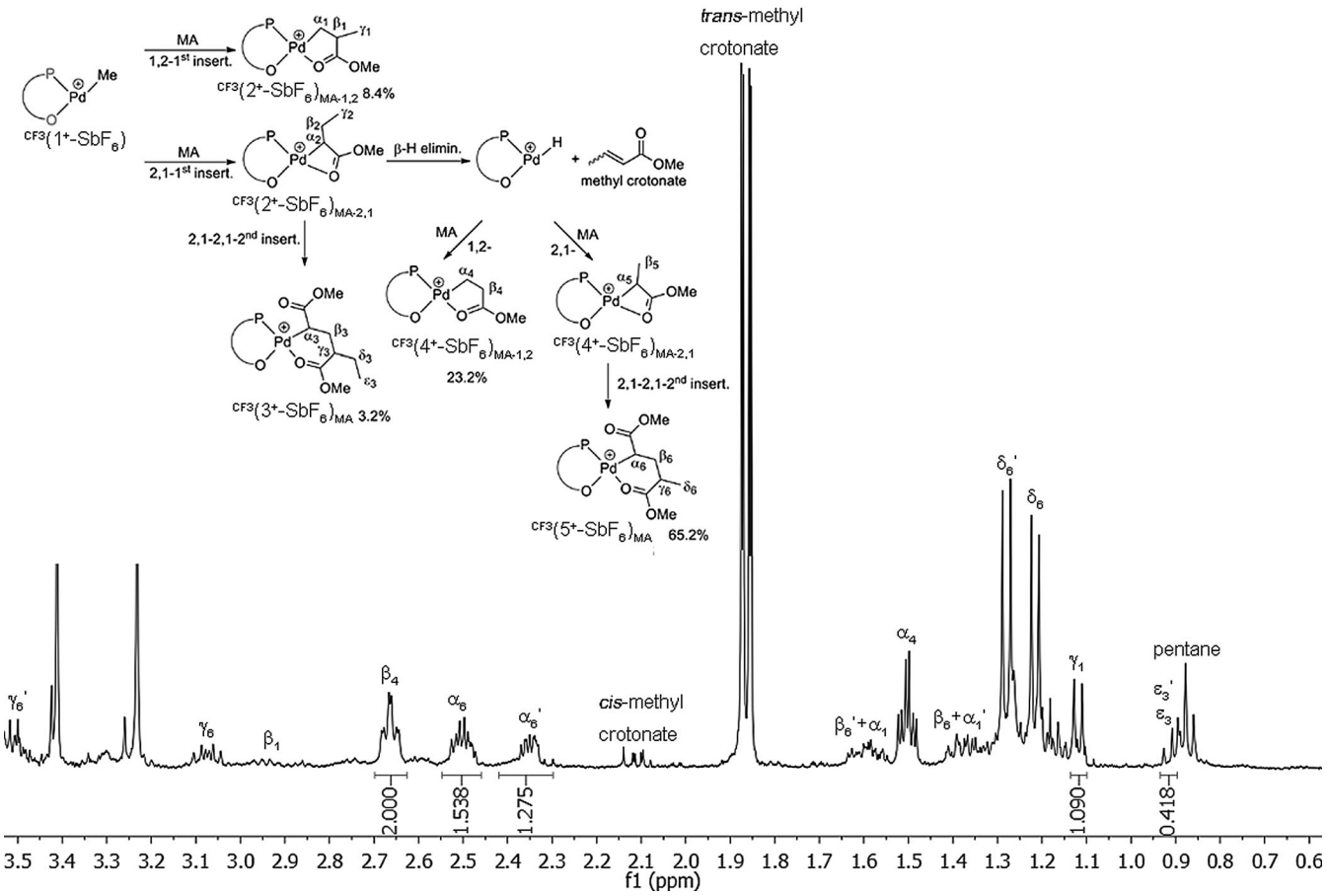


**Figure 6.** $^{1}$H NMR spectrum ($CD_2Cl_2$, 25 °C, 0–3.5 ppm) of $^{CF3}$**1**$^{+}$**-SbF$_6$** and MA (20 equiv) after 15 h at 25 °C.

ity in the first insertion product are about 7:1 and 12:1 for $^{DIPP}$**1-acetone/dmso** and $^{CF3}$**1-acetone/dmso**, respectively. In contrast, the β-H elimination rate constant $k_{\beta H\text{-}1st}$ of the 2,1-insertion product $^{X}$**2$_{MA\text{-}2,1}$** in all acetone and dmso complexes is on the same order of magnitude ($10^{-5}$ s$^{-1}$), which is much smaller than those for the cationic complexes. The first MA insertion rate constant ($k_{1st} = 3.8\times10^{-3}$ s$^{-1}$) for the phosphine–sulfonamide complex $^{CF3}$**1-dmso** is slightly larger than that of $k_{1st} = 3.2\times10^{-3}$ s$^{-1}$ for phosphinesulfonato complex $^{PSO3}$**1′-NaCl**, but the second MA insertion rate constant ($k_{2nd} = 5.1\times10^{-5}$ s$^{-1}$) for $^{CF3}$**1-dmso** is smaller than that of $k_{2nd} = 9.2\times10^{-5}$ s$^{-1}$ for $^{PSO3}$**1′-NaCl**. In addition, a second MA insertion is favored over β-H elimination for all cases, and thus $^{X}$**3$_{MA}$** is the major product after about 15 h (Scheme 6).

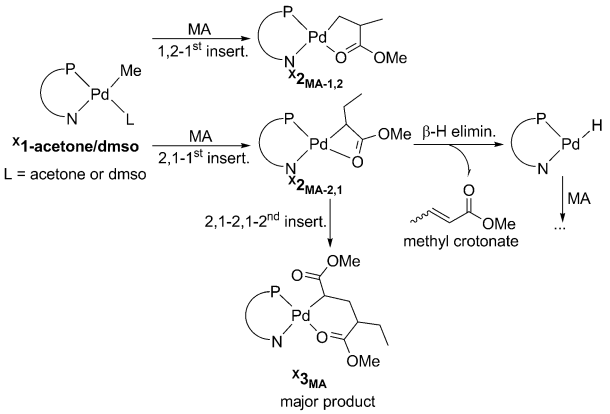


**Scheme 6.** Reaction of MA with neutral Pd$^{II}$ complexes $^{X}$**1-acetone** and $^{X}$**1-dmso**.

### *Insertion into strongly coordinated neutral complexes*

Compared with weakly coordinated acetone and dmso molecules, strongly coordinated pyridine generally impedes the pre-equilibrium reaction (**Pd**-pyridine + monomer ⇌ **Pd**-monomer + pyridine) to disfavor monomer insertion, and thus decreases the overall insertion rate of monomer (Supporting Information, Figures S54–S56). Under pseudo-first-order conditions, the observed rate constants ($k_{1st} = (1.0\text{–}50)\times10^{-7}$ s$^{-1}$) of the first 2,1 insertion of MA into the pyridine complexes $^{X}$**1-pyr** are four to five orders of magnitude smaller than those for the corresponding acetone complexes ($k_{1st} > (80\text{–}100)\times10^{-3}$ s$^{-1}$) at 25 °C (Table 3, runs 13–15).

To explore the insertion of MA into the pyridine complexes $^{X}$**1-pyr** more clearly, the same kinetic experiments were carried out at higher temperature (50 °C; Supporting Information, Fig-

ures S57–S59). The observed rate constants ($k_{1st} = (1.3–4.8) \times 10^{-5}\ s^{-1}$) of the first MA insertion at a 50 °C are about one order of magnitude higher than those at 25 °C (Table 3, runs 17–19), and are close to that for the phosphinesulfonato complex **$^{PSO3}$1′-pyr** ($k_{1st}(50\,°C) = 1.2 \times 10^{-5}\ s^{-1}$; Table 3, run 16; see Supporting Information, Figures S60 and S61), but still significantly smaller than those for corresponding acetone complexes **$^{X}$1-acetone** and dmso complexes **$^{X}$1-dmso**. In the first insertion step, the 2,1 mode is observed exclusively (Scheme 7). In addition, β-H elimination of the 2,1-insertion product is not observed at 50 °C after 15 h, except for **$^{DIPP}$2-pyr$_{MA\text{-}2,1}$** (Scheme 7). The observed β-H elimination rate constant ($k_{\beta H\text{-}1st} = 0.6 \times 10^{-5}\ s^{-1}$) of **$^{DIPP}$2-pyr$_{MA\text{-}2,1}$** is on the same order of magnitude as that of $k_{\beta H\text{-}1st} = 1.8 \times 10^{-5}\ s^{-1}$) for **$^{PSO3}$1′-pyr**. Note that we did not observe the consecutive MA insertion product for all pyridine complexes.

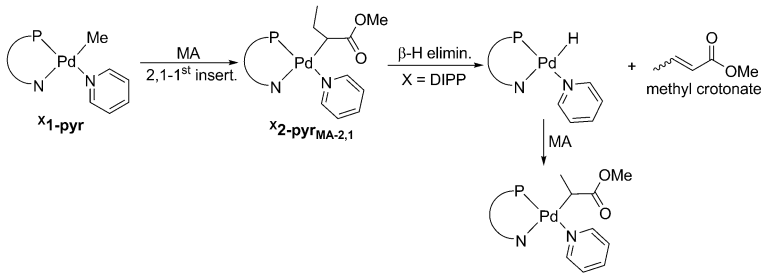


**Scheme 7.** Reaction of MA with neutral Pd$^{II}$ complexes **$^{X}$1-pyr** at 50 °C.

### Further reactivity of the isolated first, 2,1-insertion product

In the pyridine complexes **$^{H}$1-pyr** and **$^{CF3}$1-pyr**, neither β-H elimination nor second MA insertion occur in the initial 2,1-insertion products **$^{H}$2-pyr$_{MA\text{-}2,1}$** and **$^{CF3}$2-pyr$_{MA\text{-}2,1}$**. To further elucidate this observation, studies were conducted starting from the isolated 2,1-insertion product **$^{CF3}$2-pyr$_{MA\text{-}2,1}$**. Treatment of the acetone complex **$^{CF3}$1-acetone** with an excess of MA for 5 min at 25 °C ($k_{1st} > 80 \times 10^{-3}\ s^{-1}$), followed by addition of pyridine, yielded the targeted 2,1-insertion product **$^{CF3}$2-pyr$_{MA\text{-}2,1}$** (Scheme 8). In the $^1$H NMR spectrum of **$^{CF3}$2-pyr$_{MA\text{-}2,1}$**, triplets for α-H and γ-H appear at $\delta = 1.84$ ppm and $-0.10$ ppm, respectively, and two broad singlets at $\delta = 0.58$ and 1.13 ppm are assigned to β-H (Supporting Information, Figure S62). Suitable crystals of **$^{CF3}$2-pyr$_{MA\text{-}2,1}$** were isolated and analyzed by X-ray diffraction, which unambiguously proved the molecular structure of **$^{CF3}$2-pyr$_{MA\text{-}2,1}$** (cf. Supporting Information, Figure S64).[23] For the evaluation of the reactivity of **$^{CF3}$2-pyr$_{MA\text{-}2,1}$** toward MA, the behavior of an excess of MA (ca. 20 equiv) towards **$^{CF3}$2-pyr$_{MA\text{-}2,1}$** was monitored by $^1$H NMR spectroscopy at 50 °C over 15 h (Supporting Information, Figure S63). The kinetic experiment effectively confirmed that both β-H elimination and MA insertion did not take place in **$^{CF3}$2-pyr$_{MA\text{-}2,1}$**. By contrast, when the reaction of MA with **$^{CF3}$2-pyr$_{MA\text{-}2,1}$** was monitored at 95 °C, fast β-H elimination of **$^{CF3}$2-pyr$_{MA\text{-}2,1}$** was observed.

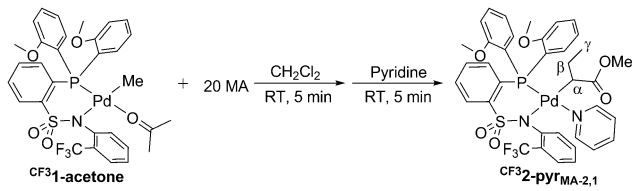


**Scheme 8.** Synthesis of initial 2,1-insertion product **$^{CF3}$2-pyr$_{MA\text{-}2,1}$**.

### Dimerization and oligomerization of ethylene

Ethylene oligomerization to form linear short-chain α-olefins has received much attention from both academia and industry over the past decades.[24] Depending on the chain length of linear α-olefins, they can be used for various purposes. For example, 1-butene, 1-hexene, and 1-octene can be employed as comonomers in ethylene copolymerization for the production of linear low-density polyethylene.[25] To date, a number of palladium(II) catalysts with various bidentate ligands such as bis-phosphine,[26] phosphine–trifluoroborate,[27] NHC–pyridine,[28a,b] phosphine–pyridine,[28c–e] bis(heterocycle)–methane,[28f] phenacyldiaryl–phosphine,[28h] and 1,10-phenanthroline[28i,j] have been reported to dimerize ethylene, with a moderate content of 1-butene. In addition, it is well-known that bidentate phosphinesulfonato Pd$^{II}$ complexes **$^{PSO3}$1′** can catalyze the polymerization of ethylene to produce linear polyethylene.[9]

#### *Ethylene dimerization catalyzed by cationic complexes*

Under pressure-reactor conditions (20 bar, 60 °C, 30 min), exposure of the cationic Pd$^{II}$ methyl complexes **$^{X}$1$^{+}$-A** to ethylene resulted in a high catalytic activity, as monitored by the ethylene mass flow. Butenes, small amounts of hexene, and very little octene were formed, as revealed by $^1$H NMR, GC, and GC-MS analysis of the reaction mixture.[29] Note that the workup procedure involved cooling of the pressure reactor to 0 °C prior to opening after the reaction, after which samples were withdrawn and analyzed. Hereby, the larger part of the butenes content is actually recorded. However, unavoidable loss of the volatile butenes will result in a somewhat overestimated value of the ratio of $C_6$ and $C_8$ to $C_4$ in Table 4.

Complexes **$^{X}$1$^{+}$-BF$_4$** showed a high activity of $6.2 \times 10^4\ h^{-1}$ for ethylene dimerization, giving butenes ($C_4$) as the major product (Table 4, runs 1–3). For different *N*-aryl substitution patterns, no apparent differences in activity were observed, but the content of $C_4$ in the short chain α-olefin product signifycantly increased in the order $CF_3$ (89.9%) > isopropyl (71.2%) > H (53.2%). This different behavior shows that the sul-

**Table 4.** Ethylene oligomerization by cationic and neutral $Pd^{II}$ phosphine–sulfonamide catalysts.[a]

| Run | Catalyst precursor | $T$ [°C] | $p_E$ [bar] | TOF[b] [$h^{-1}$] | Selectivity [%][c] $C_4$ ($\alpha$)[d] | $C_6$ | $C_8$ |
|---|---|---|---|---|---|---|---|
| 1 | $^{H}$**1**$^{+}$-$BF_4$ | 60 | 20 | 5.5 | 53.2 (99.4) | 30.8 | 16.0 |
| 2 | $^{DIPP}$**1**$^{+}$-$BF_4$ | 60 | 20 | 6.2 | 71.2 (99.7) | 22.0 | 6.8 |
| 3 | $^{CF3}$**1**$^{+}$-$BF_4$ | 60 | 20 | 6.2 | 89.9 (99.0) | 7.5 | 2.6 |
| 4 | $^{H}$**1**$^{+}$-$SbF_6$ | 60 | 20 | 4.3 | 82.7 (97.6) | 14.6 | 2.7 |
| 5 | $^{DIPP}$**1**$^{+}$-$SbF_6$ | 60 | 20 | 4.8 | 89.6 (87.7) | 8.4 | 2.0 |
| 6 | $^{CF3}$**1**$^{+}$-$SbF_6$ | 60 | 20 | 5.5 | 97.3 (92.3) | 2.4 | 0.3 |
| 7 | $^{X}$**1**-**L**[e] | 25–80 | 20 | – | oligomers | | |
| 8 | $^{CF3}$**1**$^{+}$-$BF_4$ | 60 | 5 | 3.6 | 92.2 (98.7) | 6.5 | 1.3 |
| 9 | $^{CF3}$**1**$^{+}$-$BF_4$ | 60 | 10 | 5.7 | 92.1 (99.1) | 6.6 | 1.3 |
| 10 | $^{CF3}$**1**$^{+}$-$BF_4$ | 60 | 40 | 5.7 | 90.1 (99.3) | 8.2 | 1.7 |
| 11 | $^{CF3}$**1**$^{+}$-$SbF_6$ | 60 | 5 | 3.6 | 97.3 (72.5) | 2.1 | 0.6 |
| 12 | $^{CF3}$**1**$^{+}$-$SbF_6$ | 60 | 10 | 5.2 | 97.4 (83.6) | 2.2 | 0.4 |
| 13 | $^{CF3}$**1**$^{+}$-$SbF_6$ | 60 | 40 | 4.8 | 97.7 (99.3) | 1.8 | 0.5 |
| 14 | $^{CF3}$**1**$^{+}$-$SbF_6$ | 80 | 40 | 4.8 | 96.2 (92.6) | 3.6 | 0.2 |
| 15 | $^{CF3}$**1**$^{+}$-$SbF_6$ | 40 | 40 | 3.8 | 95.8 (99.2) | 3.8 | 0.4 |

[a] Conditions: Pd (3 μmol), toluene (100 mL), 30 min, 1000 rpm. [b] Turnover frequency (TOF) = ($10^4$ × moles ethylene consumed)/(moles Pd × h). [c] Determined from the reaction solution by GC and GC-MS and $^1$H NMR. [d] $\alpha$ = amount of 1-butene in the $C_4$ dimers. [e] X = H, DIPP, $CF_3$; L = acetone, dmso, pyridine.

fonamide moiety stays coordinated to the metal center during catalysis. The amount of 1-butene is more than 99.0% in these experiments, and only traces of internal isomers are formed. With increasing ethylene pressure from 5 to 40 bar, the amount of $C_4$ and 1-butene scarcely changed for the active catalyst $^{CF3}$**1**$^{+}$-$BF_4$, although the activity was affected (Table 4, runs 3 and 8–10).

On changing the anion from $BF_4$ to $SbF_6$, a slight decrease of the activity for ethylene dimerization was observed with complexes $^{X}$**1**$^{+}$-$SbF_6$ (Table 4, runs 4–6). However, the trend of the amount of $C_4$ was in agreement with that of the $^{X}$**1**$^{+}$-$BF_4$ system. The order of the $C_4$ content is $CF_3$ (97.3%) > isopropyl (89.6%) > H (82.7%), that is, complex $^{CF3}$**1**$^{+}$-$SbF_6$ with its electron-withdrawing $CF_3$ group yields the highest content of butenes of all six cationic complexes under the same conditions. Essentially, these findings confirm that the counterion is noncoordinating and has little effect on catalytic activity. Additionally, the studies with the two different counterions mutually confirmed the trends in selectivity observed for the different phosphine–sulfonamides. In particular, with increasing ethylene pressure from 5 to 40 bar, the content of $C_4$ in the product was almost unchanged (97.3–97.7%), whereas the amount of 1-butene in the $C_4$ fraction increased significantly from 72.5 to 99.3% (Table 4, runs 6 and 11–13). This phenomenon suggests that a high pressure of ethylene can suppress the 2,1 reinsertion of the 1-butene into PdH species to generate the isomerization product 2-butene, which has also been observed in the analogous Ni catalyst system.[30] On the other hand, pressure-reactor experiments under similar conditions as in these ethylene dimerization experiments but in the presence of MA also yielded butenes as the major product (80 °C, 10 bar, 0.3 M methyl acrylate, 20 μmol, $^{CF3}$**1**$^{+}$-$SbF_6$).

### *Ethylene oligomerization catalyzed by neutral complexes*

In contrast, under pressure-reactor conditions (20 bar, 25–80 °C, 30 min), very low to no activity of the neutral $\kappa^2$-P,N $Pd^{II}$ methyl complexes $^{X}$**1-acetone/dmso/pyr** towards ethylene was monitored by mass flow. The $^1$H NMR spectra and GC analysis of the reaction solution revealed that only very little oligomer was obtained.

## Computational studies

The experimental stoichiometric and pressure-reactor studies showed that the $Pd^{II}$ phosphine–sulfonamide complexes can rapidly insert acrylate, but no polyethylene chain growth occurs for the complexes studied. To further understand this behavior, reactivities of the cationic $^{CF3}$**1**$^{+}$ and the neutral $^{CF3}$**1**, $^{H}$**1** phosphine–sulfonamide $Pd^{II}$ complexes towards ethylene (E) were investigated by DFT calculations.

### *Cationic complex $^{CF3}$**1**$^{+}$*

Concerning the free-energy profile for the first ethylene insertion into PdMe, for the κ-*O*-Pd-Me fragment $^{CF3}$**1**$^{+}$ (**A**) a reaction coordinate comprising coordination of ethylene *cis* to the oxygen atom, *cis–trans* isomerization to place ethylene *trans* to the oxygen atom, and ethylene insertion to yield the β-agostic Pd propyl complex (***O***)**β-ago-Pd-propyl** was studied (Scheme 9). In addition, for each intermediate and the insertion transition state (TS), energies for the respective κ-*N*-Pd species **B** were also calculated. For the sake of clarity, Scheme 9 contains relevant species and energies along the lowest-energy pathway (for all other geometries and energies, see Supporting Information).


**Scheme 9.** Free-energy profile [kcal mol$^{-1}$ in solvent] of the first ethylene insertion into a PdMe species to form a Pd-propyl species for $^{CF3}$**1**$^{+}$.

These calculations revealed that, for the cationic complex $^{CF3}$**1**$^{+}$, κ-*O*-coordinated species are more stable than the re-

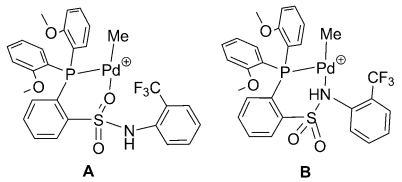

spective κ-*N*-coordinated species, the only exception being **(*O*)β-ago-Pd-propyl**, which is 1.4 kcal mol$^{-1}$ less stable than the respective **(*N*)β-ago-Pd-propyl**. Furthermore, the transition state for the isomerization of **(*O*)β-ago-Pd-propyl** to **(*N*)β-ago-Pd-propyl** is only 8.7 kcal mol$^{-1}$ higher than **(*O*)β-ago-Pd-propyl**, which makes this O/N isomerization kinetically viable. Note that the calculated overall free-energy barrier to ethylene insertion starting from cationic $^{CF3}$**1**$^{+}$ (**Pd-Me**) is only 13.1 kcal mol$^{-1}$, in agreement with the experimentally observed high catalytic activity of the $^{CF3}$**1**$^{+}$ system towards ethylene.[31]

Starting from both **(*O*)β-ago-Pd-propyl** and **(*N*)β-ago-Pd-propyl**, two competitive reactions were further considered: 1) β-H elimination in the presence of ethylene leading to propene plus **(*O*/*N*)E-*cis*-Pd-H** (Scheme 10), and 2) a second ethylene insertion into the Pd–propyl bond (Scheme 11). To better clarify the issues at hand, the energy of **(*O*)β-ago-Pd-propyl** was used as a reference point.[32]

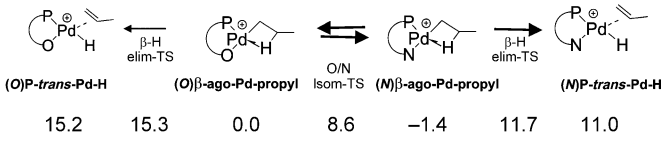


**Scheme 10.** Free-energy profile [kcal mol$^{-1}$ in solvent] of the elimination pathways from Pd-propyl for $^{CF3}$**1**$^{+}$.

The lowest free-energy pathway for β-H elimination starting from **(*O*)β-ago-Pd-propyl** lies 11.7 kcal mol$^{-1}$ higher than **(*O*)β-ago-Pd-propyl** and comprises isomerization of **(*O*)β-ago-Pd-propyl** to **(*N*)β-ago-Pd-propyl** prior to β-H elimination. In contrast, a β-H elimination starting from **(*O*)β-ago-Pd-propyl** and directly evolving into **(*O*)P-*trans*-Pd-H** requires 15.3 kcal mol$^{-1}$ (Scheme 10).

The lowest free-energy pathway for the insertion of ethylene into **(*O*)β-ago-Pd-propyl** proceeds without N/O isomerization and lies 20.9 kcal mol$^{-1}$ higher than **(*O*)β-ago-Pd-propyl** (Scheme 11). This compares to a calculated barrier for β-H elimination of 12 kcal mol$^{-1}$, in agreement with the experimental finding that $^{CF3}$**1**$^{+}$ is an ethylene dimerization catalyst.

In fact, with respect to the cationic system $^{CF3}$**1**$^{+}$, the calculations indicate that, after the first fast ethylene insertion into the PdMe catalyst precursor, the system prefers to undergo elimination instead of inserting another ethylene molecule. The formed Pd hydride complex inserts and eliminates ethylene in a fast equilibrium reaction. However, the Pd ethyl complex present in this equilibrium eventually undergoes further ethylene insertion, which ultimately results in the formation of a Pd butyl complex. Considering that a Pd propyl species is generally viewed as a proper model of the growing chain,[33] an essentially similar behavior of Pd butyl and Pd propyl species is expected, considering the competition between β-H elimination and ethylene insertion. Thus, the selective formation of 1-butene seems reasonable as long as 1-butene itself is not consumed.

Interestingly, the calculations suggest that the propensity for β-H elimination of the $^{CF3}$**1**$^{+}$ system may not primarily be related to the positive charge of the complex, but rather to the possibility of switching from O coordination to N coordination of the sulfonamide ligand to give the N-coordinated intermediate **(*N*)β-ago-Pd-propyl**, which allows for a facile β-H elimination reaction rather than a further chain-growth step (Schemes 10 and 11).

### *Neutral complexes $^{CF3}$1 and $^{H}$1*

With the aim of rationalizing the experimentally observed low activity of the neutral complexes for ethylene polymerization, the reactivity of complexes $^{CF3}$**1** and $^{H}$**1** towards ethylene was studied and compared with that of dianisyl phosphinesulfonato Pd$^{II}$ complex $^{PSO3}$**1**′ as a reference system.[34] $^{CF3}$**1** and $^{H}$**1** were chosen because the corresponding R substituents ($CF_3$, H) differ in terms of both steric and electronic effects, but the two complexes show the same behavior in producing ethylene oligomers with a low activity.

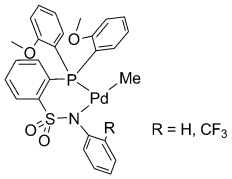


This analysis (Scheme 12) suggests that the energy profiles of ethylene insertion of the neutral sulfonamide systems $^{CF3}$**1** and $^{H}$**1** are higher than for the reference system, and the $^{CF3}$**1** system shows the highest energy in each catalytic step (i.e., intermediates and transition states). In fact, the calculated energy of ethylene coordination is 5.3 kcal mol$^{-1}$ for $^{CF3}$**1** and 0.9 kcal mol$^{-1}$ for $^{H}$**1**, as opposed to only −3.9 kcal mol$^{-1}$ for the reference system. The energy barriers of the *cis*/*trans* isomerization[35] for $^{CF3}$**1** and $^{H}$**1** are roughly 8 and 5 kcal mol$^{-1}$ higher than for the reference system, respectively, and at the same time the corresponding **E-*trans*-Pd-Me** intermediates are 7.3 and 1.6 kcal mol$^{-1}$ higher, respectively. In view of the rate-determining step of ethylene insertion, the ethylene insertion TS lies at 23.5 and 18.6 kcal mol$^{-1}$ for $^{CF3}$**1** and $^{H}$**1**, respectively, which are about 9 and 4 kcal mol$^{-1}$ higher than that of the reference system. This agrees with the experimentally observed very low activity of $^{CF3}$**1** and $^{H}$**1** towards ethylene.

To further rationalize this result, a steric and electronic analysis of $^{CF3}$**1** and $^{H}$**1** (Table 5) was performed. By comparing these

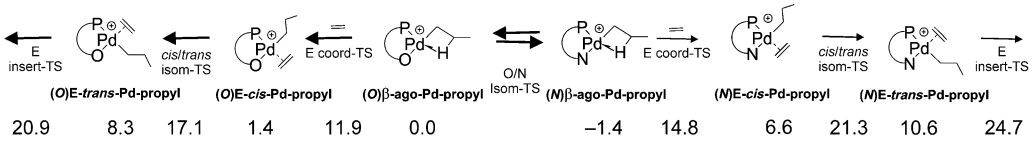


**Scheme 11.** Free-energy profile [kcal mol$^{-1}$ in solvent] of the ethylene insertion pathways from Pd-propyl for $^{CF3}$**1**$^{+}$.

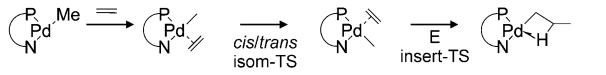


| | Pd-Me | E-*cis*-Pd-Me | | E-*trans*-Pd-Me | | β-ago-Pd-propyl |
|---|---|---|---|---|---|---|
| $^{CF3}$**1** | 0.0 | 5.3 | 19.8 | 9.1 | 23.5 | –3.3 |
| $^{H}$**1** | 0.0 | 0.9 | 16.8 | 3.4 | 18.6 | –10.4 |
| $^{PSO3}$**1**′ | 0.0 | –3.9 | 11.8 | 1.8 | 14.9 | –10.4 |

**Scheme 12.** Free-energy profile [kcal mol$^{-1}$] of the first ethylene insertion into PdMe for $^{CF3}$**1** and $^{H}$**1**.

**Table 5.** Electronic and steric analysis of Pd complexes.

| | $^{CF3}$**1** | $^{H}$**1** | Reference |
|---|---|---|---|
| Pd charge | +0.22 | +0.25 | +0.30 |
| %$V_{Bur}$ | 63.0 | 56.1 | 48.2 |

results with those reported for the reference system $^{PSO3}$**1**′, it clearly emerges that the sulfonamide complexes $^{CF3}$**1** and $^{H}$**1** are sterically more hindered at the Pd center, as indicated by the buried volume %$V_{Bur}$. Furthermore, electronic analysis indicates that they have a smaller positive charge on the Pd atom than the reference system. Notably, the $^{CF3}$**1** system features the lowest positive charge but the highest %$V_{Bur}$ ($^{CF3}$**1**, $^{H}$**1**, and $^{PSO3}$**1**′: +0.22e versus +0.25e and +0.30e; 63.0 versus 56.1 and 48.2), that is, the sulfonamide ligand affects the charge at the Pd center through the Pd–N bond, and the *N*-aryl substituent also imparts a higher steric hindrance around the metal center. The difference in the charge and in %$V_{Bur}$ between the two sulfonamide systems can be rationalized by the analysis of the geometry of $^{CF3}$**1** (Figure 7), in which an interaction between the fluorine atom of the ligand and the Pd center is established with a Pd–F distance of 2.34 Å.[36] This interaction, which stabilizes the intermediate, can account for the slightly smaller positive charge calculated for the Pd center in $^{CF3}$**1** (despite the presence of the electron-withdrawing $CF_3$ group) with respect to $^{H}$**1**.

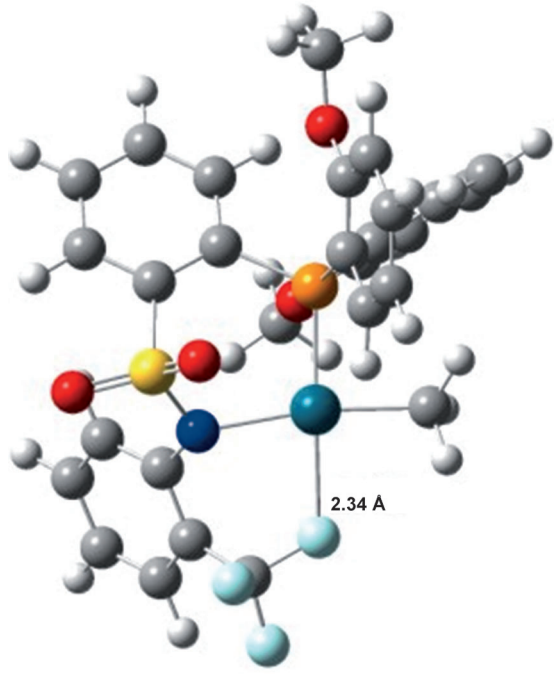


**Figure 7.** Structure of $^{CF3}$**1**. O red, P orange, N blue, S yellow, Pd green, F cyan, C gray, H white.

Despite some electronic differences between the sulfonamide and the sulfonate systems, the greater steric hindrance at the Pd center in the neutral sulfonamide catalysts $^{CF3}$**1** and $^{H}$**1** may be responsible for the experimentally observed low activity towards ethylene. This differs from the effect of steric bulk in cationic α-diimine catalysts.[37]

To test this hypothesis, ethylene insertion into the less encumbered neutral system $^{N\text{-}Me}$**1** was calculated, in which a methyl substituent is located at the nitrogen atom of the sulfonamide ligand. In agreement with this interpretation, the order of %$V_{Bur}$ is $^{CF3}$**1** (63.0) > $^{H}$1 (56.1) > $^{N\text{-}Me}$1 (51.6) > $^{PSO3}$**1**′ (48.2), and the calculated order of energy of the ethylene insertion TS is $^{CF3}$**1** (23.5) > $^{H}$1 (18.6) > $^{N\text{-}Me}$**1** (17.7) > $^{PSO3}$**1**′ (14.9).

## Conclusion

These studies on the reactivities of new cationic and neutral palladium(II) phosphine–sulfonamide complexes towards olefins suggest that:

1) The sulfonamide moiety in the cationic palladium(II) phosphine–sulfonamide complexes stays coordinated to the metal center throughout all reaction steps. There is no evidence that it only stabilizes the catalyst precursor, but the actual catalytically active species features a monodentate phosphine coordination mode.[38]
2) N coordination of the sulfonamide moiety promotes chain transfer versus chain growth. This seems to be promoted by the steric bulk of the additional organic substituents (*N*-aryl or *N*-alkyl) on the coordinating hard donor, rather than a different charge density on the central metal atom.
3) For O-coordinated species, insertion barriers and barriers of chain transfer could be potentially favorable for insertion-polymerization chain growth, providing that chain transfer can be suppressed.

This in-depth experimental and theoretical study on the phosphine–sulfonamide motif also identified decisive features of the unique neutral phosphinesulfonato motif, which is also reflected in recently reported cationic phosphine/phosphine monoxide and cationic phosphine/diethyl phosphonate complexes.[39] In addition to the unsymmetrical nature with a soft (P) and hard (O) σ-donor and likely an appropriate charge at the active site imparted by the donor characteristics of the bidentate ligand, the lack of further substituents on an O donor with their steric requirement appears to be beneficial.

## Experimental Section

### General procedures and materials

Further experimental details are given in the Supporting Information.

Unless stated otherwise, all manipulations of air- and moisture-sensitive compounds were carried out under an inert gas atmosphere by using standard glovebox and Schlenk techniques. Toluene was distilled from sodium, methylene chloride and pentane were distilled from $CaH_2$, and THF and diethyl ether ($Et_2O$) were distilled from sodium/benzophenone ketyl. Acetone p.a. and methyl acrylate (MA) were degassed by repetitive freeze–thaw cycles and used without further purification. DMSO and pyridine were purchased from Aldrich and used without further purification. $AgBF_4$ and $AgSbF_6$ were purchased from Aldrich. [PdMeCl(COD)][40] was prepared according to a literature procedure. Ethylene (3.5 grade) was purchased from Praxair. All deuterated solvents were supplied by Eurisotop.

NMR spectra were recorded on a Varian Unity Inova 400 or a Bruker Avance 400 spectrometer. $^1H$ and $^{13}C$ chemical shifts were referenced to the solvent signals. The identity and purity of palladium complexes and insertion products were established by $^1H$, $^{13}C$, $^{19}F$, and $^{31}P$ NMR spectroscopy, elemental analysis, and single-crystal X-ray diffraction. NMR assignments were confirmed by $^1H$,$^1H$ COSY, $^1H$,$^1H$ TOCSY, $^1H\{^{13}C\}$ HSQC, and $^1H\{^{13}C\}$ HMBC experiments. $^{19}F$ and $^{31}P$ NMR chemical shifts were referenced to $CFCl_3$ and 85% $H_3PO_4$, respectively. Elemental analyses were performed on an Elementar vario MICRO cube instrument. Gas chromatography (GC) was carried out on a PerkinElmer Clarus 500 instrument with autosampler and FID detection on a PerkinElmer Elite-5 (5% diphenyl-/95% dimethylpolysiloxane) Series Capillary Columns (length: 30 m, inner diameter: 0.25 mm, film thickness: 0.25 mm) by using helium as carrier gas at a flow rate of 1.5 mL min$^{-1}$. The injector temperature was 300 °C. After injection the oven was kept isothermal at 40 °C for 7 min, heated at 40 K min$^{-1}$ to 280 °C, and kept isothermal at 280 °C for 3 min.

X-ray diffraction data were collected performed at 100 K on a STOE IPDS-II diffractometer equipped with a graphite-monochromated radiation source ($\lambda = 0.71073$ Å) and an image-plate detection system. A crystal mounted on a fine glass fiber with silicon grease was employed. The selection, integration, and averaging procedure of the measured reflex intensities, the determination of the unit-cell dimensions by a least-squares fit of the $2\theta$ values, data reduction, LP correction, and space-group determination were performed with the X-Area software package delivered with the diffractometer.[41] A semiempirical absorption correction was performed. The structure was solved by direct methods (SHELXS-97), completed by difference Fourier syntheses, and refined with full-matrix least-squares techniques by using SHELXL-97 with minimization of $w\left(F_o^2 - F_c^2\right)^2$.[42] Following anisotropic refinement of all non-H atoms, ideal hydrogen positions were calculated in a isotropic riding model. The weighted $R$ factor ($wR$) and the goodness of fit $S$ were based on $F^2$; the conventional $R$ factor ($R$) was based on $F$. All scattering factors and anomalous dispersion factors were provided by the SHELXL-97 program. Hydrogen atoms were treated in a riding model. Thermal ellipsoid representations were created with ORTEP-3.[43]

CCDC 973617 (**Lb**), 973618 ($^{DIPP}$**1-Cl**), 973619 ($^{DIPP}$**(1$^+$-SbF$_6$)$_{decomp.}$**), 977700 ($^{DIPP}$**1-acetone**), 977701 ($^{CF3}$**1-dmso**), 973620 ($^{H}$**1-pyr**), 973621 ($^{DIPP}$**1-pyr**) and 973622 ($^{CF3}$**1-pyr**) contain the supplementary crystallographic data for this paper. These data can be obtained free of charge from The Cambridge Crystallographic Data Centre via www.ccdc.cam.ac.uk/data request/cif.

### Ethylene oligomerization

Oligomerization of ethylene was carried out in a 250 mL mechanically stirred (1000 rpm) stainless steel pressure reactor equipped with a heating/cooling jacket supplied by a thermostat controlled by a thermocouple dipping into the polymerization mixture. A valve controlled by a pressure transducer allowed for applying and maintaining a constant ethylene pressure. The required flow of ethylene, corresponding to ethylene consumed by polymerization, was monitored by a mass flow meter and recorded digitally. Prior to polymerization experiments, the reactor was heated under vacuum to 90 °C for at least 60 min and then brought to the desired temperature and backfilled with argon. A stock solution of the catalyst precursor in methylene chloride was prepared daily and stored in the glovebox at −30 °C. The amount required was transferred into a syringe and removed from the glovebox. 100 mL of toluene was transferred into the reactor through a cannula in a slight argon stream before the catalyst solution was injected into the reactor. After the desired reaction time, the reactor was first cooled to 0 °C and then depressurized. The reaction was quenched by adding 1 mL of methanol. The polymerization solution was immediately studied by $^1H$ NMR, GC, and GC-MS.

### Reactions with ethylene and MA

Reactions with ethylene and MA were carried out in a 250 mL mechanically stirred (1000 rpm) stainless steel pressure reactor equipped with a heating/cooling jacket supplied by a thermostat controlled by a thermocouple dipping into the polymerization mixture. A valve, controlled by a pressure transducer, allowed for applying and maintaining a constant ethylene pressure. Prior to oligomerization experiments, the reactor was heated under vacuum to 90 °C for at least 60 min, brought to the desired temperature, and backfilled with argon. A solution of MA was prepared by dissolving the desired amount of MA in toluene (50 mL total volume). 200 mg of butylated hydroxytoluene (BHT) was added to this solution before it was cannula-transferred in a slight argon stream into the reactor. A stock solution of the catalyst precursor in methylene chloride was prepared daily and stored in the glovebox at −30 °C. The amount required was transferred into a syringe, transferred out of the glovebox, and the catalyst solution was injected into the reactor. Ethylene pressure was applied, and after the desired reaction time, the reactor was first cooled to 0 °C and then depressurized. The reaction was quenched by adding 1 mL of methanol, and then three drops of polymerization solution was taken and immediately studied by $^1H$ NMR, GC, and GC-MS.

### Computational details

All DFT geometry optimizations were performed at the GGA BP86[44] level of theory with the Gaussian 09 package.[45] The electronic configuration of the systems was described by the 6-31G basis set for H, C, N, S, F, P and O, while for Pd we adopted the quasi-relativistic LANL2DZ ECP effective core potential.[46] All geometries were characterized as minimum or transition state through frequency calculations. The reported free energies were obtained through single-point energy calculations on the BP86/6-31G geometries by using the BP86 functional and the triple-ζ TZVP[47] basis set on main group atoms. Solvent effects were included with the PCM model with toluene[48] as solvent. In this BP86/TZVP electronic

energy in solvent, the thermal corrections from the gas-phase frequency calculations at the BP86/6-31G level were included.

## Acknowledgements

Z.J. is grateful to the Alexander von Humboldt Foundation for a postdoctoral research fellowship and to the University of Konstanz for a EU FP7 Marie Curie Zukunftskolleg Incoming Fellowship Programme (grant no. 291784).

**Keywords:** coordination modes · density functional calculations · dimerization · insertion · palladium

[1] a) V. C. Gibson, S. K. Spitzmesser, *Chem. Rev.* **2003**, *103*, 283; b) S. Mecking, *Angew. Chem. Int. Ed.* **2001**, *40*, 534; *Angew. Chem.* **2001**, *113*, 550; c) S. Mecking, *Coord. Chem. Rev.* **2000**, *203*, 325; d) S. D. Ittel, L. K. Johnson, M. Brookhart, *Chem. Rev.* **2000**, *100*, 1169.

[2] L. K. Johnson, C. M. Killian, M. Brookhart, *J. Am. Chem. Soc.* **1995**, *117*, 6414.

[3] a) L. Zhang, M. Brookhart, P. S. White, *Organometallics* **2006**, *25*, 1868; b) F. A. Hicks, M. Brookhart, *Organometallics* **2001**, *20*, 3217; c) C. Wang, S. Friedrich, T. R. Younkin, R. T. Li, R. H. Grubbs, D. A. Bansleben, M. W. Day, *Organometallics* **1998**, *17*, 3149.

[4] W. Keim, *Angew. Chem. Int. Ed. Engl.* **1990**, *29*, 235; *Angew. Chem.* **1990**, *102*, 251.

[5] a) S. Mecking, *Macromol. Rapid Commun.* **1999**, *20*, 139; b) B. L. Small, M. Brookhart, *J. Am. Chem. Soc.* **1998**, *120*, 7143; c) B. L. Small, M. Brookhart, A. M. A. Bennett, *J. Am. Chem. Soc.* **1998**, *120*, 4049; d) G. J. P. Britovsek, V. C. Gibson, B. S. Kimberley, P. J. Maddox, S. J. McTavish, G. A. Solan, A. J. P. White, D. J. Williams, *Chem. Commun.* **1998**, 849.

[6] a) S. Mecking, L. K. Johnson, L. Wang, M. Brookhart, *J. Am. Chem. Soc.* **1998**, *120*, 888; b) L. K. Johnson, S. Mecking, M. Brookhart, *J. Am. Chem. Soc.* **1996**, *118*, 267.

[7] E. Drent, R. van Dijk, R. van Ginkel, B. van Oort, R. I. Pugh, *Chem. Commun.* **2002**, 744.

[8] For reviews, see: a) A. Nakamura, T. M. J. Anselment, J. Claverie, B. Goodall, R. F. Jordan, S. Mecking, B. Rieger, A. Sen, P. W. N. M. van Leeuwen, K. Nozaki, *Acc. Chem. Res.* **2013**, *46*, 1438; b) A. Nakamura, S. Ito, K. Nozaki, *Chem. Rev.* **2009**, *109*, 5215; c) E. Y.-X. Chen, *Chem. Rev.* **2009**, *109*, 5157; d) A. Berkefeld, S. Mecking, *Angew. Chem. Int. Ed.* **2008**, *47*, 2538; *Angew. Chem.* **2008**, *120*, 2572.

[9] For selected examples, see: a) H. Leicht, I. Göttker-Schnetmann, S. Mecking, *Angew. Chem. Int. Ed.* **2013**, *52*, 3963; *Angew. Chem.* **2013**, *125*, 4055; b) B. Neuwald, L. Caporaso, L. Cavallo, S. Mecking, *J. Am. Chem. Soc.* **2013**, *135*, 1026; c) T. Friedberger, P. Wucher, S. Mecking, *J. Am. Chem. Soc.* **2012**, *134*, 1010; d) L. Piche, J. C. Daigle, G. Rehse, J. P. Claverie, *Chem. Eur. J.* **2012**, *18*, 3277; e) S. Ito, M. Kanazawa, K. Munakata, J. Kuoda, Y. Okumura, K. Nozaki, *J. Am. Chem. Soc.* **2011**, *133*, 1232; f) Z. Shen, R. F. Jordan, *Macromolecules* **2010**, *43*, 8706; g) T. Rünzi, D. Fröhlich, S. Mecking, *J. Am. Chem. Soc.* **2010**, *132*, 17690; h) K. Nozaki, S. Kusumoto, S. Noda, T. Kochi, L. W. Chung, K. Morokuma, *J. Am. Chem. Soc.* **2010**, *132*, 16030; i) S. Ito, K. Munakata, A. Nakamura, K. Nozaki, *J. Am. Chem. Soc.* **2009**, *131*, 14606; j) S. Noda, A. Nakamura, T. Kochi, L. W. Chung, K. Morokuma, K. Nozaki, *J. Am. Chem. Soc.* **2009**, *131*, 14088; k) D. Guironnet, P. Roesle, T. Rünzi, I. Göttker-Schnetmann, S. Mecking, *J. Am. Chem. Soc.* **2009**, *131*, 422; l) T. Kochi, S. Noda, K. Yoshimura, K. Nozaki, *J. Am. Chem. Soc.* **2007**, *129*, 8948; m) W. Weng, Z. Shen, R. F. Jordan, *J. Am. Chem. Soc.* **2007**, *129*, 15450; n) K. M. Skupov, P. R. Marella, M. Simard, G. P. A. Yap, N. Allen, D. Conner, B. L. Goodall, J. P. Claverie, *Macromol. Rapid Commun.* **2007**, *28*, 2033; o) D. K. Newsham, S. Borkar, A. Sen, D. M. Conner, B. L. Goodall, *Organometallics* **2007**, *26*, 3636.

[10] B. P. Carrow, K. Nozaki, *J. Am. Chem. Soc.* **2012**, *134*, 8802.

[11] A series of nickel complexes with $\kappa^2$-P,N coordinated phosphine-sulfonamide has been reported by Brookhart et al. to catalyze ethylene oligomerization ($7 <$ degree of polymerization $< 25$), see: J. L. Bennett, M. Brookhart, L. K. Johnson, C. M. Killian, Patent Application WO1998030610A1, **1998**.

[12] O. Pestovsky, A. Shuff, A. Bakac, *Organometallics* **2006**, *25*, 2894.

[13] J. Vela, G. R. Lief, Z. Sheng, R. F. Jordan, *Organometallics* **2007**, *26*, 6624.

[14] T. Rünzi, U. Tritschler, P. Roesle, I. Göttker-Schnetmann, H. M. Möller, L. Caporaso, A. Poater, L. Cavallo, S. Mecking, *Organometallics* **2012**, *31*, 8388.

[15] C. C. Lu, J. C. Peters, *J. Am. Chem. Soc.* **2002**, *124*, 5272.

[16] a) S. K. Bhargava, S. H. Privér, A. C. Willis, M. A. Bennett, *Organometallics* **2012**, *31*, 5561; b) J. Zhang, R. Pattacini, P. Braunstein, *Inorg. Chem.* **2009**, *48*, 11954.

[17] T. Rünzi, D. Guironnet, I. Göttker-Schnetmann, S. Mecking, *J. Am. Chem. Soc.* **2010**, *132*, 16623.

[18] a) P. Wucher, P. Roesle, L. Falivene, L. Cavallo, L. Caporaso, I. Göttker-Schnetmann, S. Mecking, *Organometallics* **2012**, *31*, 8505; b) P. Wucher, L. Caporaso, P. Roesle, F. Ragone, L. Cavallo, S. Mecking, I. Göttker-Schnetmann, *Proc. Natl. Acad. Sci. USA* **2011**, *108*, 8955; c) A. Hamada, P. Braunstein, *Organometallics* **2009**, *28*, 1688; d) A. Meduri, T. Montini, F. Ragaini, P. Fornasiero, E. Zangrando, B. Milani, *ChemCatChem* **2013**, *5*, 1170; e) V. Rosar, A. Meduri, T. Montini, F. Fini, C. Carfagna, P. Fornasiero, G. Balducci, E. Zangrando, B. Milani, *ChemCatChem* **2014**, *6*, 2403.

[19] a) B. Neuwald, L. Falivene, L. Caporaso, L. Cavallo, S. Mecking, *Chem. Eur. J.* **2013**, *19*, 17773; b) P. Wucher, V. Goldbach, S. Mecking, *Organometallics* **2013**, *32*, 4516; c) D. Guironnet, L. Caporaso, B. Neuwald, I. Göttker-Schnetmann, L. Cavallo, S. Mecking, *J. Am. Chem. Soc.* **2010**, *132*, 4418.

[20] The cationic complexes do not contain coordinated solvents, and thus the net rate constant can be assumed to be equal to the observed rate constant.

[21] Detailed assignments of these signals can be found in Table S1 of the Supporting Information.

[22] To observe the product $^{CF3}\mathbf{4}^{+}$-$\mathbf{A}_{MA\text{-}2,1}$, a full analysis was carried out after 5 h (see Figure S35 in the Supporting Information).

[23] In the crystal structure of $^{CF3}$**2-pyr**$_{MA\text{-}2,1}$, the incorporated MA moiety is disordered; hence, we cannot discuss the crystal data but provide them quantitatively as a proof and reference.

[24] a) D. S. McGuinness, *Chem. Rev.* **2011**, *111*, 2321; b) P. W. N. M. van Leeuwen, N. D. Cleḿent, M. J. L. Tschan, *Coord. Chem. Rev.* **2011**, *255*, 1499; c) T. Agapie, *Coord. Chem. Rev.* **2011**, *255*, 861; d) C. Janiak, F. Blank, *Macromol. Symp.* **2006**, *236*, 14; e) F. Speiser, P. Braunstein, L. Saussine, *Acc. Chem. Res.* **2005**, *38*, 784; f) J. Skupinska, *Chem. Rev.* **1991**, *91*, 613.

[25] a) P. W. N. N. van Leeuwen, *Homogeneous Catalysis*, Kluwer Academic, Dordrecht (The Netherlands), **2004**, p. 175; b) "Oligomerization of ethylene to higher linear $\alpha$-olefins": D. Vogt, in *Applied Homogeneous Catalysis with Organometallic Compounds, Vol. 1* (Eds.: B. Cornils, W. A. Herrmann), **1996**, Wiley-VCH, Weinheim, p. 245; c) D. E. James, *Encyclopedia of Polymer Science and Engineering, Vol. 6* (Eds.: H. F. Mark, N. M. Bikales, C. G. Overberger, G. Menges), Wiley-Interscience, New York, **1985**, p. 429.

[26] E. Drent, European Patent 0,170,311 B1, **1989**.

[27] a) Y. Kim, R. F. Jordan, *Organometallics* **2011**, *30*, 4250; b) A. L. Gott, W. E. Piers, J. L. Dutton, R. McDonald, M. Parvez, *Organometallics* **2011**, *30*, 4236.

[28] a) V. Khlebnikov, A. Meduri, H. Mueller-Bunz, T. Montini, P. Fornasiero, E. Zangrando, B. Milani, M. Albrecht, *Organometallics* **2012**, *31*, 976; b) V. Khlebnikov, A. Meduri, H. Mueller-Bunz, B. Milani, M. Albrecht, *New J. Chem.* **2012**, *36*, 1552; c) J. Flapper, H. Kooijman, M. Lutz, A. L. Spek, P. W. N. M. van Leeuwen, C. J. Elsevier, P. C. J. Kamer, *Organometallics* **2009**, *28*, 3272; d) J. Flapper, P. W. N. M. van Leeuwen, C. J. Elsevier, P. C. J. Kamer, *Organometallics* **2009**, *28*, 3264; e) J. Flapper, H. Kooijman, M. Lutz, A. L. Spek, P. W. N. M. van Leeuwen, C. J. Elsevier, P. C. J. Kamer, *Organometallics* **2009**, *28*, 1180; f) C. T. Burns, R. F. Jordan, *Organometallics* **2007**, *26*, 6726; g) M. D. Doherty, S. Trudeau, P. S. White, J. P. Morken, M. Brookhart, *Organometallics* **2007**, *26*, 1261; h) J. M. Malinoski, M. Brookhart, *Organometallics* **2003**, *22*, 5324; i) F. C. Rix, M. Brookhart, P. S. White, *J. Am. Chem. Soc.* **1996**, *118*, 4746; j) F. C. Rix, M. Brookhart, *J. Am. Chem. Soc.* **1995**, *117*, 1137.

[29] Representative $^1$H NMR spectrum and GC trace can be found in the Supporting Information; compare Figures S29 and S30.

[30] D. V. Gutsulyak, A. L. Gott, W. E. Piers, M. Parvez, *Organometallics* **2013**, *32*, 3363.

[31] The calculated energetic barrier for ethylene insertion into the Pd–Me bond of $^{CF3}\mathbf{1}^{+}$ of 13.1 kcal mol$^{-1}$ is comparable to that of 14.9 kcal mol$^{-1}$

 

calculated for the neutral dianisyl phosphinesulfonato $Pd^{II}$ complex $^{PSO3}$**1′**.

[32] a) For the chain transfer reaction, namely **(*N*)P-*trans*-Pd-H** + E → **(*N*)E-*cis*-Pd-H** + P and **(*O*)P-*trans*-Pd-H** + E → **(*O*)E-*cis*-Pd-H** + P, different routes, such as associative, dissociative, and concerted mechanisms, have been considered and were calculated. See also W. Heyndrickx, G. Occhipinti, V. R. Jensen, *Chem. Eur. J.* **2014**, *20*, 7962. b) Note that a comparison of the calculated values of energetic barriers for β-H elimination and insertion needs to take into account the different molecularities of the reactions.

[33] P. Corradini, G. Guerra, L. Cavallo, *Acc. Chem. Res.* **2004**, *37*, 231.

[34] Calculations reported here refer to the same geometries as reported in reference [19a]. However, as outlined in the Experimental Section and the Supporting Information, here we reported free energies in toluene obtained by adding the thermal corrections from gas-phase frequency analysis of the optimized geometries to the internal energies obtained from single-point calculation in the solvent.

[35] Energies of the most stable *cis–trans* isomerization TSs are reported for all systems. Energies for ethylene insertion TSs from the most stable *cis* coordination intermediate were also calculated. They are higher than the *trans* insertion TS by about 8 kcal mol$^{-1}$.

[36] D. P. Gates, S. A. Svejda, E. Oñate, C. M. Killian, L. K. Johnson, P. S. White, M. Brookhart, *Macromolecules* **2000**, *33*, 2320.

[37] The different effects of bulky substituents in cationic α-diimine catalysts and neutral sulfonamide catalysts, respectively, in ethylene polymerization essentially arise from the termination mechanism, which is bimolecular (β-H transfer) in the former and monomolecular (β-H elimination) in the latter case. Since the bimolecular TS is more spatially demanding, it is affected more by a steric hindrance around the metal center. As a consequence, bulky substituents on the diimine complexes are essential for the formation of high molecular weight polyethylene. Vice versa, for the sulfonamide complexes, steric interactions between the ligand substituents and the growing chain destabilize the insertion TS more than the elimination TS, which is reflected in the catalyst activity (see Supporting Information).

[38] Triphenylphosphine-stabilized palladium complexes have been found to catalyze ethylene dimerization to butene with low activity: a) A. Sen, T. Lai, *J. Am. Chem. Soc.* **1982**, *104*, 3520; b) A. Sen, T. Lai, *J. Am. Chem. Soc.* **1981**, *103*, 4627.

[39] N. D. Contrella, J. R. Sampson, R. F. Jordan, *Organometallics* **2014**, *33*, 3546.

[40] R. E. Rülke, J. M. Ernsting, A. L. Spek, C. J. Elsevier, P. W. N. M. van Leeuwen, K. Vrieze, *Inorg. Chem.* **1993**, *32*, 5769.

[41] X-RED version 1.31 Data Reduction Program, Stoe, Darmstadt, Germany, **2005**.

[42] a) G. M. Sheldrick, SHELXS-97 Program for Crystal Structure Analysis, University of Göttingen, Göttingen, Germany, **1997**; b) G. M. Sheldrick, SHELXL-97 Program for Crystal Structure Refinement, University of Göttingen, Göttingen, Germany, **1997**.

[43] L. J. Faruggia, ORTEP-3 V2.02 for Windows XP, University of Glasgow, Glasgow, Scotland, **2008**.

[44] a) A. D. Becke, *Phys. Rev. A* **1988**, *38*, 3098; b) J. P. Perdew, *Phys. Rev. B* **1986**, *33*, 8822; c) J. P. Perdew, *Phys. Rev. B* **1986**, *34*, 7406.

[45] M. J. Frisch et al. Gaussian 09 Revision A.1, Gaussian, Inc., Wallingford, CT, **2009**.

[46] F. Weigend, R. Ahlrichs, *Phys. Chem. Chem. Phys.* **2005**, *7*, 3297.

[47] a) T. Leininger, A. Nicklass, H. Stoll, M. Dolg, P. Schwerdtfeger, *J. Chem. Phys.* **1996**, *105*, 1052; b) W. Küchle, M. Dolg, H. Stoll, H. Preuss, *J. Chem. Phys.* **1994**, *100*, 7535; c) U. Häussermann, M. Dolg, H. Stoll, H. Preuss, *Mol. Phys.* **1993**, *78*, 1211.

[48] a) V. Barone, M. Cossi, *J. Phys. Chem. A* **1998**, *102*, 1995; b) J. Tomasi, M. Persico, *Chem. Rev.* **1994**, *94*, 2027.

Received: August 14, 2014
Published online on December 8, 2014

 